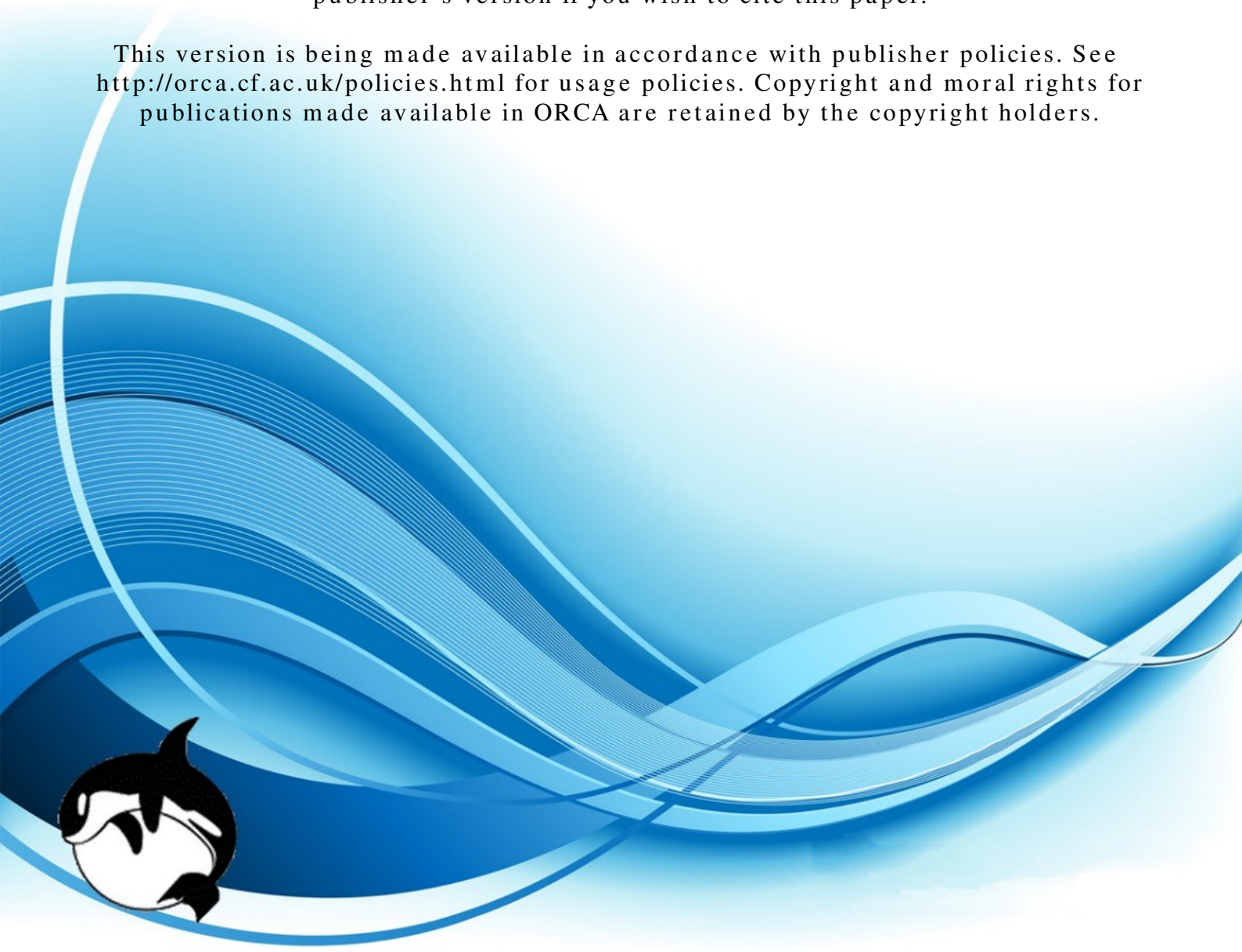

Diffusion Pruning for Rapidly and Robustly Selecting Global Correspondences using Local Isometry

GARY K.L. TAM[1,2], RALPH R. MARTIN[1], PAUL L. ROSIN[1] and YU-KUN LAI[1]
[1] Cardiff University [2] Swansea University

Finding correspondences between two surfaces is a fundamental operation in various applications in computer graphics and related fields. Candidate correspondences can be found by matching local signatures, but as they only consider local geometry, many are globally inconsistent. We provide a novel algorithm to prune a set of candidate correspondences to those most likely to be globally consistent. Our approach can handle articulated surfaces, and ones related by a deformation which is globally non-isometric, provided that the deformation is *locally* approximately isometric. Our approach uses an efficient diffusion framework, and only requires geodesic distance calculations in small neighbourhoods, unlike many existing techniques which require computation of global geodesic distances. We demonstrate that, for typical examples, our approach provides significant improvements in accuracy, yet also reduces time and memory costs by a factor of several hundred compared to existing pruning techniques. Our method is furthermore insensitive to holes, unlike many other methods.

Categories and Subject Descriptors: I.3.7 [**Computer Graphics**]: Three-Dimensional Graphics and Realism; I.3.5 [**Computer Graphics**]: Computational Geometry and Object Modeling

Additional Key Words and Phrases: 3D Geometry, Articulation, Registration, Deformation, Correspondences

ACM Reference Format:

Tam, G. K. L., Martin, R. R., Rosin, P. L., and Lai Y.-K. 2013. Diffusion Pruning for Rapidly and Robustly Selecting Global Correspondences using Local Isometry. ACM Trans. Graph. xx, y, Article nn (Month Year), 17 pages.
DOI = 10.1145/pp.qq
http://doi.acm.org/10.1145/pp.qq

This work was supported by the Engineering and Physical Sciences Research Council [grant number EP/I000100/1].

[1] School of Computer Science & Informatics, Cardiff University, UK
[2] Department of Computer Science, Swansea University, UK
Authors' addresses: G. K. L. Tam, E-mail: kltam327@gmail.com. R. R. Martin, P. L. Rosin and Y.-K. Lai, E-mail: {Ralph.Martin, Paul.Rosin, Yukun.Lai}@cs.cardiff.ac.uk.

DOI 10.1145/XXXXXXX.YYYYYYY
http://doi.acm.org/10.1145/XXXXXXX.YYYYYYY

1. INTRODUCTION

Finding correspondences between surfaces is a key operation in many applications in computer graphics and related fields. Given two surfaces identical up to pose, the task is to identify a set of point pairs, one from each surface, such that the two points in a pair correspond to the same location on each instance of the surface; this task may readily be generalised to multiple surfaces. In practice, surfaces are often represented by discrete approximations to their geometry, and more generally, the surfaces may only be alike rather than identical, so additional criteria must be used to determine what comprises a pair of corresponding points.

Various applications depend upon reliable correspondences, such as surface reconstruction from multiple scans, statistical analysis of shape spaces, sub-part identification and shape retrieval, geometry and texture transfer, and shape morphing. However, shape correspondence is a challenging problem [van Kaick et al. 2011]. Finding the most meaningful correspondences between surfaces is often application-related, and assumptions must be made regarding the type of deformation relating the surfaces, e.g. a rigid body transformation, an articulated deformation, or an approximately isometric deformation. In order to cope with non-rigid deformation, and partial matching (where part of the surface present in one exemplar is absent from the other), local signatures are often used, characterising the shape around each sample point on a surface using a set of numbers. Much effort has been made to develop robust and distinctive local signatures, but even so, sets of correspondences derived solely from local signatures typically contain many false matches—different parts of a shape can look very similar on a local scale.

Over the past decade, correspondence techniques have evolved significantly, particularly with regard to the kinds of deformation models used [Tam et al. 2013]. The most flexible assume that each vertex separately undergoes a locally affine or rigid transformation, with correspondences being found by non-rigid ICP and its variants [Allen et al. 2003; Pauly et al. 2005; Huang et al. 2008; Li et al. 2008; Li et al. 2009]. As the deformation model has high dimensionality, careful initialisation based on salient features, and sophisticated regularisation methods (e.g. assumption of small deformation, or integration of spatiotemporal information) are required. Alternative approaches are based on intrinsic properties invariant under isometric deformation, like distances and angles. Notable examples include isometric analysis [Huang et al. 2008; Ovsjanikov et al. 2010; Tevs et al. 2011], and Möbius transformation methods [Lipman and Funkhouser 2009; Kim et al. 2011]. The former explicitly assume that the deformation is a (near-)isometry; the latter allow more general deformations by using the conformal group, of which isometry is a subgroup.

Our goal in this paper is to develop a *pruning algorithm* based on intrinsic properties. A pruning step is an essential building block of many registration algorithms, and can be used to improve the results of many existing techniques. The problem to be solved is: given a set of tentative input correspondences C (e.g. derived

from local signatures or a non-rigid iterative closest point method), which contains both correct and incorrect correspondences, output a *subset* C' of these correspondences which are *globally consistent* and invariant under *isometric* deformation. Like much work in this area, we assume that vertices can be mapped one-to-one, and ignore the fact that discretisation may sample vertices at slightly different locations on each surface.

[Huang et al. 2008] pioneered a technique for this purpose, *spectral pruning*, incorporating it into a non-rigid iterative closest point algorithm for surface registration. This influential work is considered to be effective and efficient [Chang et al. 2011], and has inspired subsequent work, e.g. [Zheng et al. 2010]. Our new approach greatly improves the speed of spectral pruning and significantly reduces its memory costs, whilst also improving its accuracy. Indeed, our approach can be made fast enough for interactive applications.

Spectral pruning assumes that a single global isometry relates two instances of a deforming surface. The global nature of the assumption implies that *all* pairwise distances on a surface are preserved after such transformations. It models deformation well for much articulation and non-rigid deformation in the real world, up to some approximation. [Huang et al. 2008] uses global geodesic distances to describe the pairwise isometric consistency of correspondences. **Global geodesic distances** here refers to geodesic distances between pairs of points that can be *arbitrarily far apart* on the mesh. The use of global geodesic distances in both the modelling and pruning step in [Huang et al. 2008] leads to a result with **global consistency**, in the sense that the output correspondences are consistent throughout the whole mesh.

However, we observe that use of global geodesic distances leads to two problems:

(1) Global geodesics are slow to compute, forming a bottleneck in many otherwise good algorithms. Existing ways of alleviating this problem include pre-computation of geodesic distances [Kim et al. 2011], multi-core processing [Tevs et al. 2011], approximation [Sahillioglu and Yemez 2011] (via Dijkstra's algorithm or augmented by short-cut edge techniques [Hilaga et al. 2001]), mesh subsampling with feature saliency [Huang et al. 2008] and the use of a coarse to fine approach [Sahillioglu and Yemez 2011].

(2) Global geodesic distances do not necessarily represent the deformation well. Holes, noise and non-isometric deformation (e.g. near joints in articulated models) all affect the computation of geodesic distances. Existing solutions to alleviate this problem include the use of diffusion distances [Bronstein et al. 2010], biharmonic distances [Lipman et al. 2010] which are somewhat shape-aware, and fuzzy geodesic measures [Sun et al. 2010] which emphasise local geodesic distances.

The above two problems motivate the following question and corresponding contributions of this paper:

> Are **local geodesic distances** a better basis for a **globally consistent** pruning technique?

Here, we mean by *local* that we only consider geodesic distances to points within a small neighbourhood of a chosen point. There are two reasons for expecting an affirmative answer. Obviously, only considering local geodesics should be faster than computing long range geodesic distances. More subtly, the longer the paths considered on the mesh, the more likely some local distortion or hole (due to missing data) is to make a change in the geodesic distance between a pair of corresponding points. This invalidates the assumption of globally isometric consistency. On the other hand, good correspondences are often locally and isometrically consistent. Using local geodesic distances still takes account of this requirement.

Our key idea is that using global geodesic distances is not the only way to enforce global consistency. Instead, it can be *robustly inferred* from good correspondences through *diffusion*. This is similar to the idea of diffusion distances [Bronstein et al. 2010] but we apply the diffusion framework in a different and novel way, *in the space of correspondences of non-rigid surfaces*. We first use local geodesic distances to define local isometric consistency as a probability measure. In the diffusion framework, one can consider a particle jumping around a network of correspondences, with a higher chance of the particle jumping to positions where correspondences respect local isometry. In the limit of an infinite number of jumps, the stationary probability distribution defines a confidence measure of global consistency. We use this measure as a basis for a greedy pruning strategy.

The use of mostly local geodesic distances to obtain globally consistent correspondences may seem counter-intuitive. It might seem that accuracy should drop, and the results may not be globally consistent. However, the use of local isometry allows the method to better handle cases where there is locally isometric (but not globally isometric) deformation, for example near joints of articulated models. The use of a diffusion technique provides robustness, as it does not rely on global geodesic distances but *multiple paths of locally isometrically consistent correspondences* to infer global consistency. In general, diffusion analysis works well for datasets with noise and small random perturbations [Lafon and Lee 2006]; the analysis measures the average 'connectivity'. The same applies to diffusion distances, which can much better handle holes (i.e. gaps, due to missing data) on non-rigid surfaces than geodesic distances [Rosman et al. 2010].

Our novel approach can be several hundred times *faster* than the well known spectral pruning method [Huang et al. 2008], while using several hundred times *less memory*, allowing machines with moderate resources to quickly handle large meshes. Nevertheless, as we relax the deformation assumption to local isometry, the pruned results are also better, in terms of *accuracy* and *coverage*, for models undergoing articulation, for locally-isometric deformation, and for models with holes, as we demonstrate in our experiments.

Section 2 discusses related work. Section 3 outlines spectral pruning and the motivation of our approach, while Section 4 gives our technique in detail. Section 5 evaluates our technique. Section 6 discusses limitations and finally, Section 7 concludes the paper.

2. RELATED WORK

Finding correspondences between two surfaces has a long history. Two recent surveys [van Kaick et al. 2011; Tam et al. 2013] give a detailed account of many techniques. We briefly summarise some of the main papers related to our work.

2.1 Non-rigid surfaces and correspondences

2.1.1 *Features and Signatures.* Using features and signatures to find sparse correspondences between surfaces has been well-studied. Notable examples include spin images [Johnson and Hebert 1999], integral invariants [Gelfand et al. 2005], geometric hashing [Gal and Cohen-Or 2006], slippage features [Bokeloh et al. 2008], and SHOT signatures [Tombari et al. 2010]. They have also been adopted for non-rigid shape matching, and have further driven the development of signatures for the non-rigid case, like extremities [Zhang et al. 2008] and heat kernel signatures [Sun et al. 2009].

Such features and signatures are usually based on local properties, and therefore are relatively insensitive to global issues such as holes and outliers, but their use does not ensure global consistency. Further pruning [Gelfand et al. 2005; Funkhouser and Shilane 2006; Zhang et al. 2008] is usually required to provide reliable correspondences.

2.1.2 *Registration techniques.* Many non-rigid registration techniques have been developed, inspired by rigid registration techniques [Besl and McKay 1992; Chen and Medioni 1991]. Some deformation model must be assumed, e.g. small non-rigid deformation [Pauly et al. 2005; Brown and Rusinkiewicz 2007], articulation [Allen et al. 2003], piecewise rigidity [Chang and Zwicker 2008; 2009] or locally rigid or affine deformation [Huang et al. 2008; Li et al. 2008; Li et al. 2009]. Such techniques often require sophisticated regularisation. Some require good initial alignment estimates or a sequence of frames as input.

2.1.3 *Intrinsic techniques.* Intrinsic techniques based on the idea of isometric deformation, and which are thus based on distances or angles, have become a recent research focus. They assume that the distance between two vertices on one shape is the same as the distance between the two corresponding vertices on another shape. There are various ways to establish correspondences under this assumption, depending on the metric being used. These metrics include geodesic distances [Anguelov et al. 2004; Huang et al. 2008; Tevs et al. 2009; Tevs et al. 2011] and diffusion distances [Bronstein et al. 2010]. Other techniques transform the problem into an embedding space where the metrics become Euclidean, and then use eigenfunctions for establishing correspondences. These include multi-dimensional scaling [Jain and Zhang 2006], spectral embedding of the Laplacian [Mateus et al. 2008], and diffusion embedding [Sharma and Horaud 2010]. In a similar spirit, [Bronstein et al. 2006] and [Bronstein et al. 2010] use generalised multi-dimensional scaling and the Gromov-Hausdorff distance to embed one mesh directly into another. However, these algorithms may only find a local minimum if not carefully initialised. Recently, the study of harmonic bases obtained from the surface Laplace-Beltrami operator has led to success in establishing correspondence maps. Notable works include [Ovsjanikov et al. 2012] which introduces a new functional representation for correspondences, [Kovnatsky et al. 2013] which uses approximate joint diagonalization to compute coupled harmonic bases and [Pokrass et al. 2013] which uses sparse modelling to infer global correspondences from regions. Another important idea is the use of Möbius transformations [Lipman and Funkhouser 2009; Kim et al. 2011]. The isometry group is a subgroup of the Möbius (conformal, angle-preserving) group. Working in the conformal domain provides stronger constraints for correspondences while allowing greater flexibility for deformations. All existing works assume a single *global* isometry between the surface instances.

Our work has a similar basis, but we show that it is possible to use *mostly local* geodesic distances to improve global correspondence consistency: one can restrict the computation of geodesic distances to a local disc, as long as most good isometric correspondences are linked in a graph structure (which may have several connected components). This allows us to replace the assumption of global isometry by one based on *local isometry*, and simultaneously reduce the computation required. We use this as a basis for a new diffusion pruning technique, inspired by, but much more efficient than, spectral pruning [Huang et al. 2008].

2.2 Spectral Analysis

The use of spectral graph theory [Chung 1997] to establish correspondences is not new [Forsyth and Ponce 2002]. In this paper, we start with a spectral matching technique [Leordeanu and Hebert 2005] which has been extensively analysed [Leordeanu et al. 2012]. It has found wide use in computer graphics and related areas, e.g. for finding symmetric components in images [Chertok and Keller 2010], as the basis for a recent probabilistic correspondence approach [Egozi et al. 2013], for establishing correspondences between non-rigid surfaces [Huang et al. 2008] and for space-time skeletons [Zheng et al. 2010].

In this paper, we apply a diffusion framework [Coifman and Lafon 2006] to correspondence analysis. Diffusion analysis, which is also based on spectral graph theory, investigates graph properties from a local to global perspective. A number of recent works have successfully applied this framework for various purposes in mesh processing, including [Sun et al. 2009; Ovsjanikov et al. 2010; Mémoli 2011] who study the kernel arising from a converging mesh Laplacian operator on a surface, leading to the definition of diffusion distances on a mesh and an isometric one-point matching technique. It has also been used to determine symmetry [Lipman et al. 2010] and for co-segmentation [Sidi et al. 2011].

Perhaps the most relevant work to ours is [Kim et al. 2012] which applies the diffusion framework to find a consistent set of 'fuzzy correspondences' across a collection of shapes under an assumption of global isometry. Our technique, however, focuses on the *space of point correspondences between two non-rigid deforming surfaces* and shows that global consistency of correspondences between the two surfaces can be inferred via local isometry. Since our technique is a *pruning* technique, we mainly focus on comparing our approach to that in [Huang et al. 2008], for non-rigid surface correspondences.

3. REVIEW OF SPECTRAL PRUNING

Since our idea is closely related to spectral pruning [Leordeanu and Hebert 2005; Huang et al. 2008], we briefly review and analyse the technique, using a 2D toy example. Figure 1a shows two 'surfaces' (actually two polylines) with source points s_{1-6} and target points t_{1-6}. The two surfaces are related by a *globally non-isometric deformation*—each edge segment has grown longer by a small factor in the target. Such deformation is typical near joints in articulated models. We presume some other method has been used to determine the 12 input correspondences (C) shown; in this particular case each source point s_i happens to be associated with two points on the target surface (one of which is the desired target point t_i, and another is some other mismatching point t_j). The numbers on the edges in Figure 1a are used to identify these correspondences in the rest of Figure 1.

Spectral pruning [Leordeanu and Hebert 2005] models the pairwise relationships between the input correspondences by building a matrix K of size $|C| \times |C|$. Each non-zero element $K(a, b)$ describes the extent to which two correspondences a, b are in globally isometric agreement, defined by [Huang et al. 2008] as the ratio of the geodesic distances between the end-points of the two correspondences (see Section 4.2). The largest eigenvector of this matrix gives a confidence value describing the extent to which every correspondence belongs to a single consistent cluster, determined by a single global isometry.

The matrix can be interpreted using spectral graph theory [Chung 1997]. These correspondences form a weighted graph in which correspondences (e.g. a, b) form the nodes and a non-zero entry

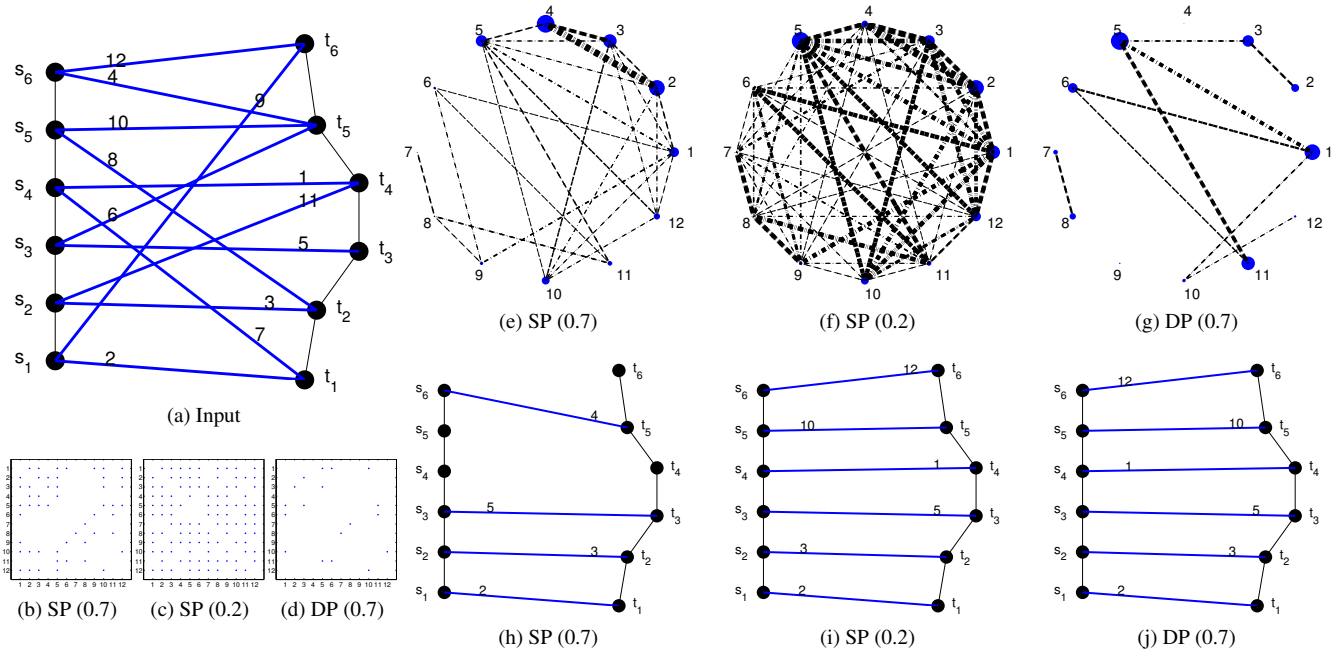

Fig. 1. Toy example demonstrating performance of spectral pruning (SP) and diffusion pruning (DP). (a): input correspondences. (b)–(d): sparse matrices model the pairwise isometry relationships between correspondences, using two different values of c_0 for SP, and one for DP; DP here uses adjacent nodes as the local neighbourhoods. (e)–(g): matrices as graph structures. Sizes of nodes indicate relative ranks of confidence values. Width of connecting lines indicates strength of pairwise isometric consistency. (h)–(j): correspondence results determined from (e)–(g).

$K(a, b)$ defines the edge weight (and thus an edge) between them. Considering pairwise relationships between *all* correspondences would result in a fully filled matrix, which would be excessive in a real problem. As described in [Leordeanu and Hebert 2005; Huang et al. 2008], one can sparsify the matrix by considering only strong relationships, i.e. any entries below a certain threshold c_0 are set to zero, removing weaker edges from the graph. This helps to improve efficiency if the deformation is truly a global isometry. However, if it is not, pruning may lead to incorrect determination of correspondences—many weaker edges which may help support a more consistent solution may have been discarded.

Figure 1b shows the matrix obtained by setting a threshold $c_0 = 0.7$ as suggested by [Huang et al. 2008], while Figure 1e shows the correspondence relationship graph for this value. The dot size for each correspondence shows the associated confidence value, and the width of each connecting edge shows the strength of the pairwise global isometric relationship.

We make two observations. Firstly, the neighbourhoods of correspondences in the spectral domain (i.e. the graph), *differ* from the neighbourhoods in the geometric domain. Whenever the two geodesic distances in a pair of correspondences differ by only a small amount, no matter how far apart they are in the geometric domain, they will form a neighbourhood. This is useful in modelling a *globally* isometrically consistent solution. The disadvantage is that, for non-rigid surfaces, agreement of long geodesic distances may not accurately reflect true correspondence relationships, especially for geodesics that run through articulating joints and other non-isometrically deforming regions. Such areas might only locally preserve isometry. This reduces the chances of finding correct correspondences in the presence of such regions.

To illustrate this, consider Figures 1e and 1h. Correspondence 4 is identified as a good one, with the highest confidence value. In terms of global isometric consistency, the geodesic distances between s_1 and s_6, and between t_1 and t_5, have highest consistency. There is also a strong isometric relationship with correspondences $5, 3, 2$. However, if correspondence 4 is included in the result, correspondences 10 and 12 conflict and cannot be selected.

One way to improve this situation is to use a less restrictive threshold, e.g. by setting $c_0 = 0.2$. Correspondence 5 then becomes the strongest correspondence because of its pairwise isometric relationship with all other correspondences (see Figure 1i). However, this results in a much denser similarity matrix (Figures 1c, 1f). In general, suppose that each point on the surface has several, say $q > 0$, candidate correspondences. The number of correspondences C is then $O(nq)$, where n is the number of mesh points. The algorithm in [Huang et al. 2008] has a memory cost $O(|C|^2) = O(n^2q^2)$ to store K.

Secondly, we also observe that the use of global geodesic distances imposes a heavy computational burden when the number of correspondences is large. Given $O(nq)$ correspondences, and the need for exact geodesic distance computation from every point to all other points on the mesh (for both surfaces), this approach needs $O(n^{2.5} \log n)$ time on average (the worst case being $O(n^3 \log n)$ [Surazhsky et al. 2005]) and $O(n^2)$ storage. This is prohibitive for large meshes, so most correspondence techniques based on geodesic computation down-sample the meshes to reduce n (perhaps to a few hundred vertices [Tevs et al. 2009; Tevs et al. 2011]), or reduce both n and q using saliency measures [Huang et al. 2008], or do both.

4. OVERVIEW

The above analysis motivates us to consider *local* geodesic distances instead of global geodesic distances. The former are, in general, more reliable in terms of modelling isometric deformation and in terms of computational efficiency [Lipman et al. 2010]. The disadvantage is that we now face a challenge to ensure global consistency of the retained correspondences. Our idea is to infer global consistency from local isometric consistency through diffusion. This is similar to computing diffusion distances on mesh points [Bronstein et al. 2010]. Here we apply the diffusion framework [Coifman and Lafon 2006] to the set of correspondences.

We proceed as follows. We first compute geodesic distances within a small local neighbourhood of each point defined by a set radius. We then build a sparse relationship matrix based on local isometric consistency. As in spectral pruning, we also compute a confidence score, but in terms of probabilities given by the diffusion framework. To reduce conflicts between correspondences, we analyse the confidence values from a global perspective. The computed confidence score is based on the assumption made by the diffusion framework that all correspondences are connected into one single graph. There are reasons that this assumption may not be met, which we consider further later. In such cases, the confidence score is then valid up to individual connected components only. We use a sophisticated greedy pruning procedure to ensure that all output correspondences are globally consistent.

Using our previous example, Figure 1d shows the matrix obtained by our technique for threshold value $c_0 = 0.7$ (cf. Figure 1b). We use adjacent vertices to define local neighbourhoods. Our much sparser graph and results are shown in Figures 1g and 1j; these are determined using less time and reduced storage.

We now formally state the problem to be solved, before explaining each step in turn. Let S and T be two surfaces and C a set of input correspondences. Our goal is to return a large set of globally consistent correspondences $C' \subset C$ that, at the same time, respect local isometry. C' should be a one-to-one vertex mapping. Our algorithm also outputs a probability value $\pi(a)$ for each correspondence $a \in C'$, which can be used as a confidence measure in downstream applications.

We now consider the steps in detail.

4.1 Geodesic Distance Precomputation

First, we define local distances through geodesic discs. Given a mesh surface M with n vertices, we let G_k^δ be a geodesic disc of vertices centred on vertex k, i.e. a set of vertices satisfying $G_k^\delta = \{v | d_g(v,k) \leq \delta D\}$, where $v \in M$, $d_g(v,k)$ is the geodesic distance between v and k, δ is a user-defined ratio and D is the diameter of the mesh (the greatest geodesic distance between any two vertices). We can quickly approximate D using the furthest sampling scheme [Peyré and Cohen 2006] and Dijkstra's algorithm, in time $O(n \log n)$. Unless stated otherwise, all $d_g(v,k)$ are computed using the exact algorithm in [Surazhsky et al. 2005]. Computation of all geodesic distances from a single vertex is a slow process with average complexity $O(n^{1.5} \log n)$. By restricting the computation to a small local neighbourhood G_k^δ, computation times are greatly reduced. Let m be the average number of vertices in G_k^δ, which can be approximately determined from the surface area A: $m \approx 2\Delta^2 \pi n / A \ll n$, where $\Delta = \delta D$ is the absolute disc size. The overall complexity for all vertices becomes $O(nm^{1.5} \log m)$.

4.2 Pairwise Local Isometry

We next model pairwise local isometry by building a matrix K. Two correspondences $a = (s_i, t_u)$ and $b = (s_j, t_v)$, $s_i, s_j \in S$ and $t_u, t_v \in T$, are related to each other if they meet both the isometric consistency and locality requirements. Isometric consistency k_{ab} of a and b requires similarity of the geodesic distances $d_g(s_i, s_j)$ and $d_g(t_u, t_v)$ between their corresponding pairs of end-points on the two surfaces (Eqns. 1, 2). The locality requirement ensures that only correspondences related by short geodesic distances are considered (Eqn. 3):

$$k_{ab} = \min\left(\frac{d_g(s_i,s_j)}{d_g(t_u,t_v)}, \frac{d_g(t_u,t_v)}{d_g(s_i,s_j)}\right), \tag{1}$$

$$k_{ab} \geq c_0, \tag{2}$$

$$s_j \in G_{s_i}^\delta \text{ and } t_v \in G_{t_u}^\delta. \tag{3}$$

Eqn. 1 ensures that $0 \leq k_{ab} \leq 1$, while Eqn. 2 requires k_{ab} to be at least c_0 for isometric consistency, where $0 < c_0 < 1$. If the consistency is lower than c_0 we simply assume these correspondences are unrelated. This has the effect of sparsifying K (see Section 2.2). The same basic idea is also used in [Huang et al. 2008], but we introduce the extra constraint in Eqn. 3, restricting related correspondences to ones where both ends fall into the local geodesic discs around the end points of the other correspondence. (Since a geodesic is symmetric, Eqn. 3 can be rewritten as $s_i \in G_{s_j}^\delta$ and $t_u \in G_{t_v}^\delta$.) This ensures that we only consider correspondences that are *locally* isometric—consistent as determined by local geodesics. Correspondences not satisfying the locality constraint are removed and do not contribute to the sparse symmetric matrix K, whose elements are given by:

$$K(a,b) = \left\{ \begin{array}{cc} (\frac{k_{ab}-c_0}{1-c_0})^2 & \text{if } a \neq b, \text{and (2), (3) are satisfied} \\ 0 & \text{otherwise} \end{array} \right\} \tag{4}$$

$c_0 = 0.7$ is a good choice of threshold [Huang et al. 2008] balancing the geodesic distance differences due to e.g. articulation, and the need for isometric consistency; we consider the effects of varying c_0 in our experiments. The complexity of building and storing K is approximately $O(|C|^2 2\Delta^2 \pi / A) = O(nq^2 m)$, which depends on the total number of correspondences $|C| = O(nq)$ and the number of correspondences that fall within each local disc $|C| 2\Delta^2 \pi / A = O(qm)$. Local correspondences can be accessed in $O(1)$ time using a hash structure, created in Section 4.1.

4.3 Diffusion Framework

We now use a diffusion framework [Coifman and Lafon 2006] on K to compute a confidence score $\pi(a)$ for each correspondence $a \in C$. K is a sparse similarity matrix which is symmetric, positivity-preserving and positive semi-definite. From a graph-theoretic point of view, (C, K) defines a graph in which correspondences C form the nodes and (a, b) defines an edge if $K(a,b)$ is non-zero, $\forall a, b \in C$. $K(a, \cdot)$ defines a neighbourhood for a, and $K(a,b)$ defines the numerical significance of the relation. K can be renormalised to a row stochastic Markov matrix P:

$$P(a,b) = K(a,b)/d(a), \quad \text{where}$$
$$d(a) = \sum_b K(a,b). \tag{5}$$

Normalising $\sum_b P(a,b) = \mathbf{1}$ allows P to be viewed as the transition kernel of a Markov chain on C. From a data analysis viewpoint, $P(a,b)$ represents the probability of transition from node a

to b in one time step, and P^t defines the transition probability from a to b in t time steps.

The main advantage of this diffusion framework is that we can run the chain forward in time. Taking higher powers of P as t increases *integrates* the local isometry information, telling us more about the global isometric consistency of C. Assume for now that the graph is connected (Section 4.4 will discuss when the graph may be disconnected and how we handle it). There is a stationary distribution $\pi(a) = P^{t\to\infty}(a,b)\beta(a)$ for any arbitrary initial distribution β. $\pi(a)$ is the unconditional or average probability of the random walk reaching a. Correspondences a with large $\pi(a)$ are usually located near the centres of clusters in the graph because there are more paths for them to reach nearby correspondences that are locally isometrically consistent.

In a similar way to how [Huang et al. 2008; Leordeanu and Hebert 2005] produce a single strongly-related global cluster, $\pi(a)$ can be used as confidence values to rank globally consistent correspondences. It can be shown that the square of the first eigenvector ψ_0 of the symmetrised version of P is exactly the stationary distribution, i.e., $\psi_0^2(a) = \pi(a)$ (see Appendix in [Coifman and Lafon 2006]). Whilst [Huang et al. 2008; Leordeanu and Hebert 2005] need to solve a sparse eigenproblem, the stationary distribution of the diffusion framework can be efficiently computed as $\pi(a) = d(a)/\sum_{b\in C} d(b)$. Thus, we require *neither* eigen-decomposition *nor* power-iteration to obtain eigenvectors. The complexity of computing $\pi(a)$ is linear in the number of non-zero entries in K, so is very efficient, particularly as K is very sparse.

The above Markov process is also related to the *diffusion distance*, defined as $D_t(a,b)^2 = |P^t(a,\cdot) - P^t(b,\cdot)|^2 = |\Psi_t(a) - \Psi_t(b)|$, where $\Psi_t = \lambda_i^t\psi_i$ and (λ_i^t, ψ_i) are the ordered eigenvalues and eigenvectors of the symmetrised version of P^t (excluding the first, largest eigenvector) [Coifman and Lafon 2006]. The diffusion distance measures the connectivity in the graph (C, K), through the induced embedding Ψ_t, with small values indicating a large number of paths connecting a and b and a large probability of transition from a to b. Whilst it is possible to use diffusion distances to analyse clusters, we find that the stationary distribution can itself be reliably used as the basis for an efficient pruning algorithm.

4.4 Globally Consistent Locally Isometric Pruning

Maximising the total confidence score and non-conflicting correspondences does not necessarily mean that the resulting correspondences are globally consistent and locally isometric. This is due to the fact that the confidence scores are inferred from local isometry. In Section 4.3, we pointed out that the diffusion framework assumes all correspondences are connected to one another via small geodesic discs. There are two reasons why the graph may be disconnected or nearly disconnected: either δ may be set too small, or c_0 may be set too high. In either case, insufficient good correspondences will remain to form paths for a particle to reach *all* other correspondences in a chain in the diffusion framework. These correspondences form clusters in the spectral domain—the diffusion distance between correspondences within a cluster is small, but is large between clusters. The stationary distribution will infer a separate 'global' consistency for each cluster independently. These clusters may not be consistent in a global sense. We thus use a further procedure to ensure *all* output correspondences are mutually consistent.

Referring back to Figure 1g, correspondences 7 and 8 form a small disjoint graph and cluster, due to the use of a small value for δ. These two correspondences are removed from the result not only because they share the same end points as correspondences 2 and 3, but also because they are not locally isometrically consistent with correspondences 5 and 1, which have higher confidence scores.

4.4.1 *Algorithm Overview.* Our pruning procedure (see Algorithm 1) is a greedy algorithm. It iteratively selects the correspondence $a \in C$ with the highest confidence score $\pi(a)$ and examines whether it can be validly included in C', classifying it as one of three cases:

C1 Both end-points of a fall in the geodesic discs of some already accepted correspondences.

C2 Both end-points of a fall outside the geodesic discs of any accepted correspondences.

C3 Only one end-point of a falls in the geodesic discs of some accepted correspondences.

We proceed as follows. If its local isometric consistency can be assessed in relation to some accepted correspondences, a clear acceptance or rejection decision can be made (C1), otherwise, the correspondence is either checked for global isometric consistency (C2), or delayed until more good correspondences are accepted (C3). Details are given below.

4.4.2 *Details and Rationale.* Given C (the input correspondences), c_0 (a consistency threshold), δ (the size of the geodesic discs relative to the surface's geodesic diameter) and $\pi(a)\ \forall a \in C$ (confidence scores), the algorithm computes a set of output correspondences C' which are c_0-locally isometric and globally consistent. There are two phases: initialisation and pruning.

During initialisation, the correspondence a with the highest score is added to C' (lines 1-2) because, in general, it has the largest local isometric consistency support—higher $\pi(a)$ in the diffusion framework indicates that there are more paths for the particle to jump around a larger set of correspondences that respect local isometry, and is usually located at the centre of the strongest cluster in the graph where more such paths are available (see Section 4.3). The algorithm further creates two lists: NEWSEEDS (line 3) and DELAY (line 4), used for handling clusters of correspondences in the case of a disconnected graph. NEWSEEDS stores accepted correspondences which have been verified by global geodesic distances; they form the centres of new clusters. DELAY stores correspondences which cannot be immediately verified by local isometric consistency.

The algorithm then begins the greedy pruning phase. The correspondence a with the next highest $\pi(a)$ is removed from C (line 7), and is determined to belong to one of three cases:

C1 Both end points of correspondence a lie in the local geodesic discs of *some* accepted correspondences $b \in B \subset C'$ (line 10). This simple case can be checked quickly. We accept a if Eqns. 1–3 are satisfied $\forall b \in B$ (line 12), and reject it otherwise.

C2 Neither end point of a lies in the geodesic disc of *any* accepted correspondences. This happens when there are clusters of correspondences arising due to a disconnected graph. Whether a should be included in C' depends on global information. We use an approximate geodesic check (using Dijkstra's algorithm) with a relaxed threshold to determine its global isometric consistency with respect to existing accepted clusters (line 17). Eqn. 6 is used to determine such approximate global geodesic distances; see lines 3, 17, and 20.

$$s_j \in G^1_{s_i} \text{ and } t_v \in G^1_{t_u}. \tag{6}$$

Algorithm 1 Compute locally isometric and globally consistent C'

Input: δ // size of geodesic discs, relative to diameter
c_0 // consistency threshold
C // input raw correspondences
$\pi(a)\ \forall a \in C$ // confidence scores for C
Output: C' // output correspondences

Initialisation
1: $a = (s_i, t_u) \leftarrow \arg\max_{b \in C}(\pi(b))$
2: $C' \leftarrow \{a\}, C \leftarrow C \setminus \{a\}$
3: NEWSEEDS $\leftarrow \{a\}$, compute $G^1_{s_i}, G^1_{t_u}$
// $G^1_{s_i}, G^1_{t_u}$ are global geodesic distance from s_i and t_u
4: DELAY $\leftarrow \emptyset$
Pruning
5: **while** $|C| > 0$ **do**
6: $a = (s_i, t_u) \leftarrow \arg\max_{c \in C}(\pi(c))$
7: $C \leftarrow C \setminus \{a\}$ // default: reject
8: $B_1 \leftarrow \{b \in C' : b = (s_j, t_v), s_j \in G^\delta_{s_i}\}$
9: $B_2 \leftarrow \{b \in C' : b = (s_j, t_v), t_v \in G^\delta_{t_u}\}$
10: $B \leftarrow B_1 \bigcap B_2$
11: **if** $|B| > 0$ **and** $|B| \,/\, \max(|B_1|, |B_2|) > 0.5$ **then**
C1
12: **if** $k_{ab} \geq c_0, \forall b \in B$, with $G^\delta_{s_j}, G^\delta_{t_v}$ **then**
13: $C' \leftarrow C' \bigcup \{a\}$ // accept, meet Eqns. 1–3
14: $C \leftarrow C \bigcup$ DELAY, DELAY $\leftarrow \emptyset$ // re-analyse
15: **end if**
16: **else if** $|B1| = |B2| = 0$ **then**
C2
17: **if** $k_{ab} \geq 0.7, \forall b \in$ NEWSEEDS, with $G^1_{s_j}, G^1_{t_v}$ **then**
18: $C' \leftarrow C' \bigcup \{a\}$ // accept, meet Eqns. 1,2,6
19: NEWSEEDS $\leftarrow$ NEWSEEDS $\bigcup \{a\}$
20: compute global $G^1_{s_i}, G^1_{t_u}$ for $a = (s_i, t_u)$
21: $C \leftarrow C \bigcup$ DELAY, DELAY $\leftarrow \emptyset$ // re-analyse
22: **end if**
23: **else**
C3
24: DELAY $\leftarrow$ DELAY $\bigcup \{a\}$ // delay
25: **end if**
26: **end while**

An approximate check may be used, as the assessment of a before other good correspondences indicates that $\pi(a)$ is higher. Since $\pi(a)$ is computed by integration of local isometry, this indicates a large support of isometrically-related correspondences around a. However, these clusters are not necessarily adjacent to each other (e.g. two rigid parts of an articulating limb forming two clusters of correspondences), and long geodesics are not reliable. We therefore use Dijkstra's algorithm to compute the approximation and use a relaxed threshold $c_0 = 0.7$ (as suggested by [Huang et al. 2008]).

If a meets the requirements in Eqns. 1, 2, 6, we accept it into the NEWSEEDS list (line 19), for use as the centre of a new cluster of good correspondences, using the same rationale as for choosing the correspondence with the highest $\pi(a)$ during initialisation. To ensure global consistency, the validity of potential new seeds will later be checked against accepted correspondences in NEWSEEDS, including a. Therefore, it is a good time to compute global geodesic distances from both end points of a to all other vertices (line 20).

This step is inspired by the global consistency check in [Huang et al. 2008]. In [Huang et al. 2008], *all* accepted correspondences must satisfy Eqns. 1, 2, 6 globally. The advantage of our check over the one in [Huang et al. 2008] is that global geodesics are only computed for important correspondences (NEWSEEDS). Evaluation (line 17) is done against accepted seeds only—the centres of clusters, not *all* accepted correspondences, and is therefore less restrictive.

The number of times case C2 occurs is relatively low (typically $\approx 0.01\%$–$2\% \times |C|$); it depends on the connectivity of good correspondences as well as the disc size δ and the consistency threshold c_0. For $\delta \geq 0.1$ and $c_0 \leq 0.4$, C2 often becomes unnecessary and the correspondence a can be accepted directly because most correspondences are connected together and $\pi(a)$ models global consistency well.

C3 Only one end point of a new correspondence is found in the geodesic discs of *some* accepted correspondences (i.e., either $|B1| > 0, |B2| = 0$ or $|B1| = 0, |B2| > 0$). These correspondences may be good (but slightly shifted) or totally incorrect. Thus, we defer a decision until later and keep them in the DELAY list (line 24). The rationale is to evaluate them later when there are more accepted correspondences to judge them against. Therefore, whenever a correspondence is accepted (line 14, 21), we move correspondences from the DELAY list back to C for re-analysis.

This greedy algorithm stops when no more correspondences remain in C. All correspondences left in the DELAY list at this stage are discarded as they are potentially incorrect. (Our experiments have shown that most correspondences left in the DELAY list are incorrect or are not c_0-isometrically consistent by this stage). The algorithm must terminate, because at every iteration one correspondence from C is either accepted, rejected or delayed. Correspondences in the DELAY list will be re-analysed only when a correspondence is accepted indicating that C is strictly smaller. The worst case complexity of this step is $O(|C|^2 + kn \log n)$ where k is the number of correspondences in the NEWSEEDS list. $O(n \log n)$ time is needed to compute a global geodesic using Dijkstra's algorithm. The pruning step is slower than that in [Huang et al. 2008] ($O(|C|) = O(nq)$) because of the re-analysis of correspondences in the DELAY list. However, this is still much faster than precomputation of all global geodesics.

4.5 Efficient Global Coherence-based Optimisation

Certain input correspondences in C may share the same end points and hence conflict. Though our pruning step in Section 4.4 can handle this problem, it is quicker to first remove them using a global coherence-based optimisation step, as follows.

Under the assumption that the output correspondences should be a partial one-to-one mapping, pruning correspondences can be viewed as maximising the number of non-conflicting correspondences whilst maximising the total sum of confidence scores. This can be posed as a *max-flow min-cost problem*. This could in principle be solved by first finding a set of solutions that maximise flow (the number of non-conflicting correspondences) in the network and then picking the one that minimises the total cost (maximise total confidence). Here, we use a more efficient implementation.

We set up a network as follows: a source node is created for every vertex of the source mesh, and similarly for the target mesh. An edge connecting the respective source and target nodes is added for every raw input correspondence a. The non-negative cost of the edge is $\max_{b \in C}(\pi(b)) - \pi(a)$. We further add two nodes (the network source and sink) and connect them by additional edges to all the source and target nodes respectively. Finally, we set the total flow to the number of source vertices and set the capacity of all

the edges to one. We solve this max-flow min-cost problem using the network simplex algorithm [Ahuja et al. 1993], and remove all correspondences whose edges have zero flow.

The complexity of this step is $O((E\log(V))(E+V\log(V)))$ where $E=|C|+2n$ and $V=2n+2$ are the numbers of edges and vertices in the flow graph. We use an open source implementation [Dezso et al. 2011] of the network simplex algorithm, which can process a sparse network with 100000 nodes in around 10 seconds. The problem can also be converted into a bipartite graph matching problem, and solved by the Hungarian algorithm, but this approach performed worse in testing, as it cannot take advantage of the sparse connectivity of the graph.

In general, this step removes many globally conflicting correspondences. On moderate-sized models, it reduces the greedy pruning time by a factor of three and increases the number of correct correspondences by 1–2%.

5. EXPERIMENTAL RESULTS

Let S and T be two surfaces for which correspondences are to be pruned. In our experiments, public datasets with ground truth correspondences are used—see Sections 5.1 and 5.2. The method in [Huang et al. 2008] and our proposed technique are both *pruning* techniques, and as such assume that some good correspondences exist in the input set. To perform our experiments, we generated sets of input correspondences C controlled by two parameters $|C|$ and $|G|$: the total number of correspondences, and the number of random ground truth correspondences added to ensure that at least some good correspondences were present in the data. The correspondence generation procedure is as follows:

(1) We first computed a signature for each vertex of the two surfaces S and T, obtained by concatenating two sets of SHOT signatures [Tombari et al. 2010] with ball radius $2\times$ and $5\times$ the average mesh edge length. Such a signature provides good performance.

(2) For each vertex on surface S, we computed the q best matches on T according to similarity of signatures ($q=1$ by default). We did the same for surface T, and combined the two sets to obtain a set H (without duplicates).

(3) Again ensuring no duplicates, $|G|$ ground truth correspondences were selected and added to the dataset.

(4) Finally $|C|-|G|-|H|$ unique random correspondences were generated (most will be incorrect and represent errors), making up the input correspondence set C.

We used SHOT signatures as they perform better [Tombari et al. 2010] than spin images [Johnson and Hebert 1999] which have previously been frequently used for finding correspondences in articulated models. Using only correspondences from SHOT signature matches, however, means that there were few correct correspondences in non-rigidly deforming areas in the input correspondences. Also, pruning techniques were often used in non-rigid iterative closest point algorithms [Huang et al. 2008] where good correspondences can be found in non-rigidly deforming areas. Introducing G allowed us to better evaluate the relative performance of our method and spectral pruning in such areas.

We evaluated our method in scenarios involving articulated deformation (Section 5.1) and non-isometric deformation (Section 5.2). Memory consumption and speed were considered in Section 5.3. We further evaluated our techniques under certain difficult conditions, including the presence of holes (Section 5.4), handles (Section 5.5) and noise (Section 5.6). We applied our technique to the SCAPE dataset which involves reconstructed human body models from real scanned data in different poses (Section 5.7). We also used our technique to provided further understanding of existing techniques (Section 5.8).

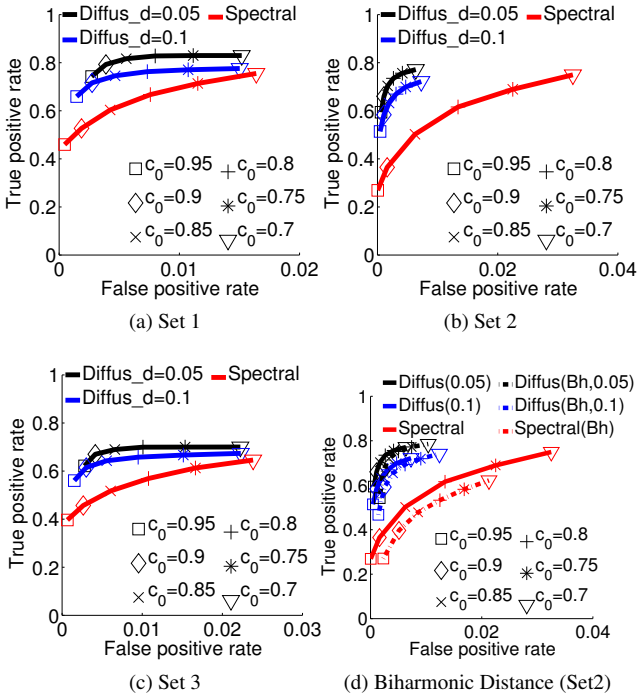

(a) Set 1 (b) Set 2

(c) Set 3 (d) Biharmonic Distance (Set2)

Fig. 2. Average ROC curves for 122 pairs of models from the TOSCA dataset with about 5000 vertices. All sets contain 10000 correspondences. On average, (a) there were 1778 correct correspondences in Set 1 according to ground truth; (b) 2763 correct in Set 2; and (c) 1313 correct in Set 3. Set 1 and Set 3 were based on SHOT signatures, designed for matching rigidly transforming surfaces. Set 1 allowed only one reciprocal correspondence for each vertex, whereas Set 3 allowed multiple matches for each vertex. Additional ground truth correspondences were added to Set 2, ensuring some good correspondences were present in the non-rigidly deforming areas. (d) further compares the use of geodesic distances and biharmonic (Bh) distances using Set 2 as an example.

5.1 Articulated models

We first evaluated the ability of our method to prune correspondences between articulated models: most parts of the body undergo approximately piecewise rigid deformation except near joint areas. Many papers have considered such mostly-isometric deformation. We used the publicly available TOSCA dataset [Bronstein et al. 2008] as it provides ground truth information for all vertices. We compared the method in [Huang et al. 2008] and our pruning techniques using (i) receiver operating characteristic (ROC) curves, which plot true positive against false positive rate with varying c_0, (ii) visual inspection, which shows the coverage and quality of correspondence results, and (iii) K-ring deviation, which measures how far (in term of K-rings) any retained incorrect correspondences deviate from the ground truth. The ROC curves are based on the exact vertex correspondences provided by the ground truth data.

5.1.1 *Small models.* Because of its high memory and time requirements, spectral pruning cannot be directly applied to large

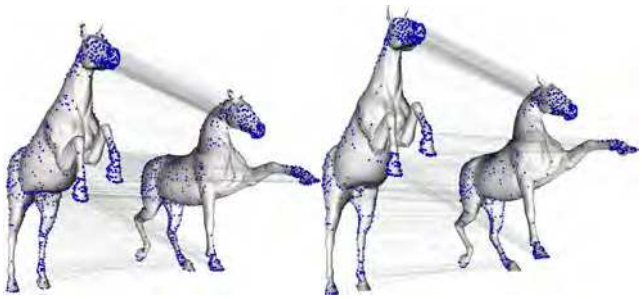

(a) DP (Set 1) $c_0 = 0.7, \delta = 0.05$ (b) DP (Set 1) $c_0 = 0.9, \delta = 0.05$

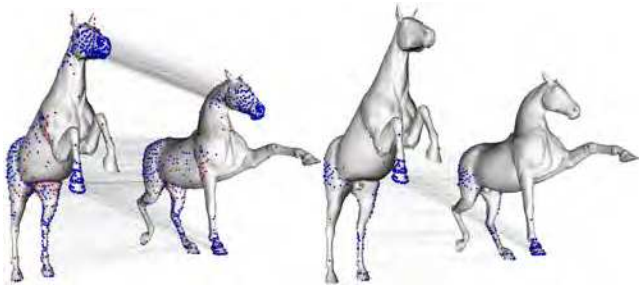

(c) SP (Set 1) $c_0 = 0.7$ (d) SP (Set 1) $c_0 = 0.9$

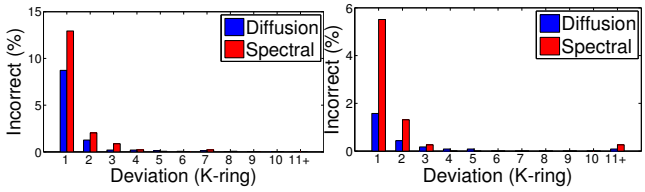

(e) Set 1 $c_0 = 0.7$ (f) Set 1 $c_0 = 0.9$

Fig. 3. Visual comparison of results of diffusion pruning (DP) and spectral pruning (SP) on small model–horse–Set 1 (a)-(f), TOSCA dataset [Bronstein et al. 2008]. Blue and red spheres show correct and incorrect correspondences. Histograms plot the percentage of incorrect correspondences against K-ring deviation from ground truth. (Shorter bars, and fewer bars on the right, are better.)

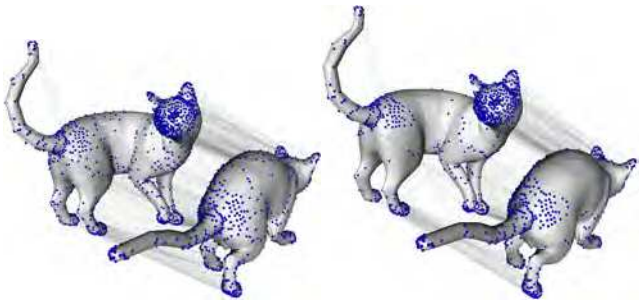

(a) DP (Set 2) $c_0 = 0.7, \delta = 0.05$ (b) DP (Set 2) $c_0 = 0.9, \delta = 0.05$

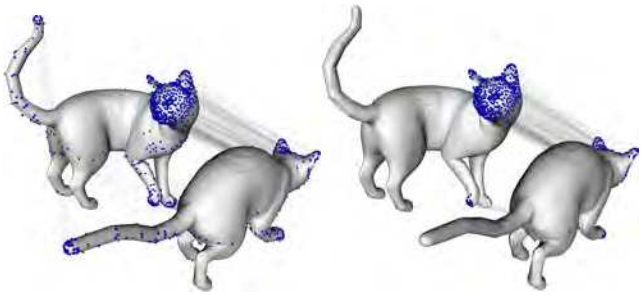

(c) SP (Set 2) $c_0 = 0.7$ (d) SP (Set 2) $c_0 = 0.9$

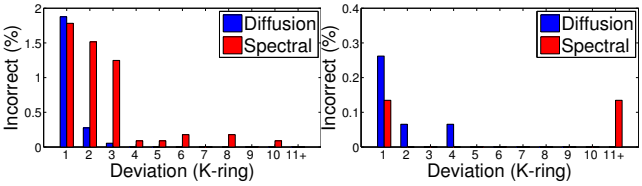

(e) Set 2 $c_0 = 0.7$ (f) Set 2 $c_0 = 0.9$

Fig. 4. Visual comparison of results of diffusion pruning (DP) and spectral pruning (SP) on small model–cat–Set 2 (a)-(f), TOSCA dataset [Bronstein et al. 2008]. Blue and red spheres show correct and incorrect correspondences. Histograms plot the percentage of incorrect correspondences against K-ring deviation from ground truth.

meshes. Therefore, we first downsampled one model in each category to 5000 vertices using *qslim* [Garland and Heckbert 1997], and propagated the changes to the other models in order to preserve the ground truth information in the dataset. Some original TOSCA models have disconnected components and/or flipped normals, and *qslim* occasionally generates non-manifold vertices on the down-sampled models. After excluding these, we obtained 55 models. We took all possible pairs in each category, resulting in 122 pairs of models. For each pair, three sets of correspondences were generated using parameters:
Set 1: $|C| = 10000$, $|G| = 0$,
Set 2: $|C| = 10000$, $|G| = 1000$,
Set 3: $|C| = |H| = 10000$ where $q \approx |C|/n$
(see Section 5). Set 1 allowed only one reciprocal correspondence for each vertex, where Set 3 allowed multiple matches for each vertex. Additional ground truth correspondences were added to Set 2. Between these 122 model pairs, on average, there were 1778 correct correspondences in Set 1, 2763 in Set 2 and 1313 in Set 3 (according to the ground truth). We used two ratios of $\delta = \{0.05, 0.1\}$ to define geodesic discs. To compute the ROC curves, we varied the threshold $c_0 = \{0.7, 0.75, 0.8, 0.85, 0.9, 0.95\}$; $c_0 = 0.7$ is the suggested threshold for spectral pruning.

Figures 2a and 2b show the average ROC curves for the 122 model pairs. Our technique outperformed spectral pruning, giving a higher true positive rate for the same false positive rate. Small geodesic discs generally produced better results for our technique. As the fraction of correct correspondences increased in the input, our technique showed greater improvement.

We visually analysed the distribution and quality of the results. Figures 3a–3d (horse) and Figure 4a–4d (cat) show two models undergoing large articulation. Here we used $\delta = 0.05$. Since the SHOT signature is designed for rigid surfaces, most of the good correspondences in Set 1 were located on rigid parts. Our technique retained these clusters of correspondences. Figures 3c and 3d show that the spectral technique does worse, and misses many good correspondences due to inconsistence on global isometry. In Set 2, apart from correspondences in rigid areas, additional correspondences were retained in the non-rigid areas. Our technique has retained accurate correspondences in certain non-isometrically de-

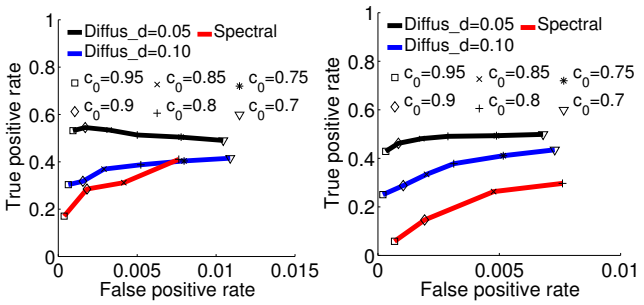

(a) Set 1 (b) Set 2

Fig. 5. Comparison of ROC curves for a large mesh (centaurs, 10000 vertices). Set 1 and Set 2 contain 30000 correspondences, 3017 and 5020 are correct according to ground truth.

forming regions (e.g. the body and legs of the cat). Again, spectral pruning failed to retain good correspondences in these regions when using the same setting for c_0. The histograms show the K-ring deviation from ground truth of retained incorrect correspondences. Our technique had fewer, and better, retained incorrect correspondences (shorter bars, and bars weighted to the left).

Several important surface distances have been proposed in recent years, including commute time distances [Fouss et al. 2007], diffusion distances [Bronstein et al. 2010] and biharmonic distances [Lipman et al. 2010]. Here, we provide a further comparison to biharmonic distances as it has been shown to be superior, in terms of shape awareness and robustness to topological change and noise, than the others for certain applications [Lipman et al. 2010]. We used exact computation of biharmonic distances to avoid approximation issues. Figure 2d shows that, in general, in our diffusion pruning techniques, local geodesic distances performed a little better than biharmonic distances. Spectral pruning also performed better when using geodesic distances.

5.1.2 *Medium-sized models.* We evaluated our method on a pair of medium-sized models of centaurs. Again, we down-sampled the model from 50000 vertices to 10000 vertices to enable comparison with spectral pruning. We generated two sets of correspondences using parameters:
Set 1: $|C| = 30000$, $|G| = 0$,
Set 2: $|C| = 30000$, $|G| = 2000$
(see Section 5). Sets 1 and 2 contain 3017 and 5020 correct correspondences.

Figure 5 shows the same trends as for small models. Our technique was more accurate than spectral pruning except in the case of Set 1 with $\delta = 0.1, c_0 = 0.8$, where it was similar. A smaller geodesic disc of $\delta = 0.05$ gave better results than $\delta = 0.1$. Note that we were unable to obtain results for spectral pruning when $c_0 < 0.8$ due to its high memory requirements.

The visual comparison in Figure 6 shows that our technique retains more good correspondences evenly spread across the whole surface. The spectral technique pruned away too many correspondences. The histograms also show that any incorrect correspondences that were retained by our technique are closer to the ground truth.

Note that the true positive rates should not be compared between the Set 1 and Set 2 of Figures 2 and 5. In Set 2, the added correct correspondences G mostly lie in non-rigidly deforming areas, making Set 2 a much more challenging case. Figure 6 provides a clearer picture. In Set 1, most correspondences were located in locally rigid regions (e.g. heads, back, rigid parts of limbs). In Set 2 more correspondences were in the non-rigid deforming parts (e.g. the stomach, back legs). Comparing Figures 6a and 6b shows that our technique was able to obtain good correspondences in these regions.

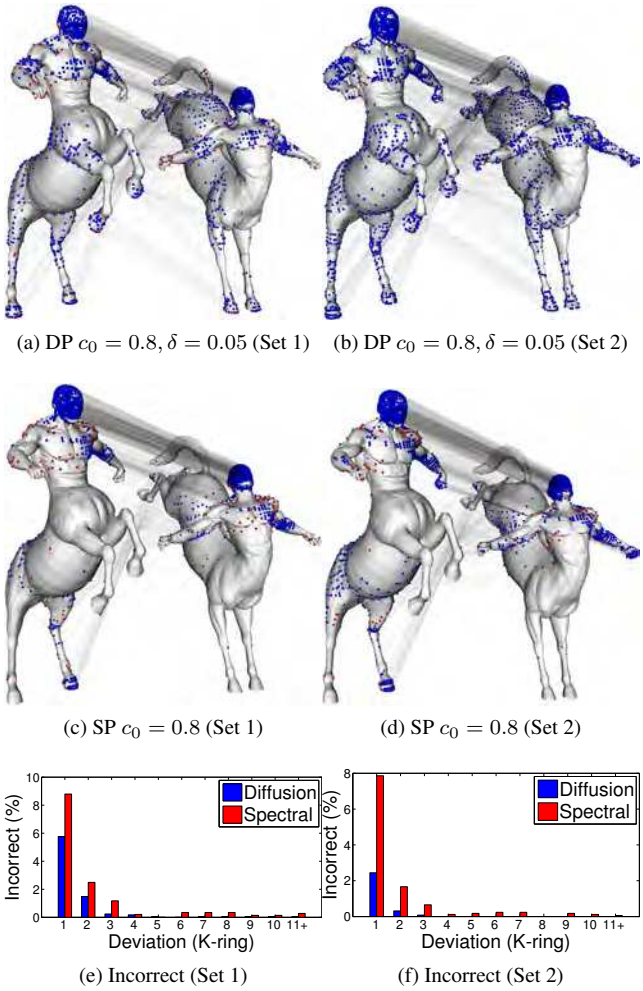

(a) DP $c_0 = 0.8, \delta = 0.05$ (Set 1) (b) DP $c_0 = 0.8, \delta = 0.05$ (Set 2)

(c) SP $c_0 = 0.8$ (Set 1) (d) SP $c_0 = 0.8$ (Set 2)

(e) Incorrect (Set 1) (f) Incorrect (Set 2)

Fig. 6. Visual comparison of results of diffusion pruning (DP) and spectral pruning (SP) on medium-sized meshes, TOSCA dataset [Bronstein et al. 2008]. Blue and red spheres are respectively correct and incorrect correspondences. Histograms plot the percentage of incorrect correspondences against K-ring deviation from ground truth.

In summary, these experiments show that pruning based on global geodesic distances does not model articulation well, especially around joints where non-isometric deformation occurs. Using small radius geodesic discs better model these regions and our technique is able to retain more accurate correspondences where models undergo articulation. With a larger number of good correspondences in the input, our technique achieves greater consistency of retained correspondences and improved accuracy of results.

5.2 Globally non-isometric deformation

We next evaluated pruning ability on meshes undergoing globally non-isometric deformation, using the face dataset from [Sumner

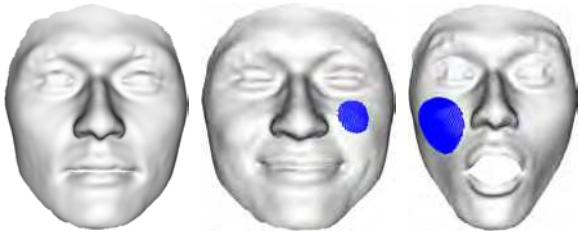

(a) Reference (b) Smile (c) Surprise

Fig. 7. Three meshes from the face dataset [Sumner and Popović 2004]. Disc sizes of $\delta = 0.05, 0.1$ are indicated to enable the reader to see how large they are relative to the whole face. Vertex count: 29299.

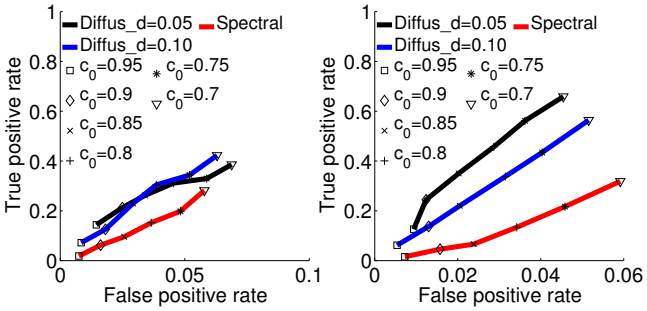

(a) Set 1 (b) Set 2

Fig. 8. Comparison of ROC curves for non-isometrically deforming meshes. Set 1 contained 10093 correspondences with 710 correct according to ground truth; Set 2 contained 10065 and 2056 correct.

and Popović 2004] (created by [Vlasic et al. 2004]). In this data, a reference face template (Figure 7a) was aligned with different 3D face scans (e.g. Figures 7b and 7c). Again, we used this dataset as it provides ground truth correspondences.

First, we evaluated pruning ability using faces showing a smile (Figure 7b) and surprise (Figure 7c). Two sets of input correspondences were generated (see Section 5):
Set 1: $|C| = 31299$, $|G| = 2000$
Set 2: $|C| = 37299$, $|G| = 8000$.
We further randomly downsampled Set 1 (to $|C| = 10093$) and Set 2 (to $|C| = 10065$), in which 710 and 2056 correspondences were correct, to enable spectral pruning to run to conclusion in reasonable time. We used 2 different disc ratios $\delta = \{0.05, 0.1\}$. Results are shown in Figure 8.

The ROC curves in Figure 8a indicate that our technique provided similar results for $\delta = 0.05, 0.1$. When $c_0 \leq 0.8$ the results with $\delta = 0.1$ outperformed those with $\delta = 0.05$. We believed the cause to be that when there were only a few sparse correct correspondences, our technique cannot connect them together with small discs, and so was unable to establish meaningful consistency across the surface. For $\delta = 0.1$ a balance was achieved between locality of modelling of isometric deformation and connecting good (and near-good) correspondences together, providing better results when $c_0 \leq 0.8$. Nevertheless, the performance of our technique was still better than spectral pruning in both cases. Given sufficient good correspondences in the input set, as in Figure 8b, our technique performed better than spectral pruning for any δ; $\delta = 0.05$ provided the best performance, and locally isometric deformation was modelled well.

Figure 9 further analysed the results visually. Globally non-isometric deformation occurs around the eyes and jaw. Our technique still provided good correspondences in these areas whilst spectral pruning was unable to cope with the deformation. The histograms show that the incorrect correspondences retained by our technique were both fewer and closer to correct ground truth correspondences.

Surprisingly, neither technique produced good correspondences around the nose region (Figure 9). The nose region is well-known for its rigidity and stability in different facial expressions and has been used for face recognition [Chang et al. 2006]. Zooming in to the nose areas (Figure 10) revealed that there was in fact subtle non-isometric deformation, as shown by the shading of polygons, and our best explanation is that the ground truth data may possibly be in error in this region—despite many correspondences being flagged as incorrect (red), they may be good correspondences in terms of isometry.

Given a set of one-to-one input correspondences for all vertices, our technique can be used to identify regions which are *not* c_0-locally isometric deforming: there were no returned correspondences in such regions. We used *all* ground truth data to define a set of one-to-one correspondences ($|C| = 29299$) for the reference face (Figure 7a) and surprise face (Figure 7c), and used them as input to our technique. In Figure 11a, the blue shading indicates regions where correspondences were returned. We observed several areas such as the lower lip and brows where no correspondences wee found, using settings of $c_0 = 0.7$, indicating non-isometric deformation as shown in detail in Figure 12. (Figures 12c-12d show the lip region using $c_0 = 0.1$. The vertices without the blue shading visualise the non-local isometric deformation—see Figure 11a).

Spectral pruning failed to provide any results even after 2 days of computation. Our method took 794s for $c_0 = 0.7$, and 718s for $c_0 = 0.1$. The additional time required by $c_0 = 0.7$, a strong threshold for non-isometric deformation, is due to invocations of the C2 step in our algorithm, which required extra computations of global geodesic distances (see Section 4.4.2).

We also observed one horizontal line of missing correspondences from left to right; this line exists even at $c_0 = 0.1$ (Figure 11b). We highlight these correspondences in Figure 11c. It turns out that these correspondences are all misaligned due to incorrect sequencing of vertices in the original file (input correspondences are generated by assuming that the reference face was deformed into the surprise face while topology and vertex id remain the same). Our technique identified this incorrect assumption concerning the reference and surprise pair. No such problem exists between the smile and surprise faces. (This dataset from [Sumner and Popović 2004] is not originally intended for evaluating *point* correspondences. This ground truth error does not affect the integrity of the results in [Sumner and Popović 2004] which are based on *triangle* correspondences).

In summary, these experiments show that our technique is able to handle locally-isometric deformation. The correspondences it retains are more accurate than those retained by spectral pruning. The experiments show the usefulness and robustness of our technique, and its ability to handle large meshes, models with a large hole, and large sets of correspondences.

5.3 Memory consumption and speed

Our method and spectral pruning were both implemented in Matlab on a machine with two Intel Xeon 2.67GHz processors and 12GB memory. All reported timings used one Matlab thread. We show the time taken and percentage of matrix filled ('Fill') for the exper-

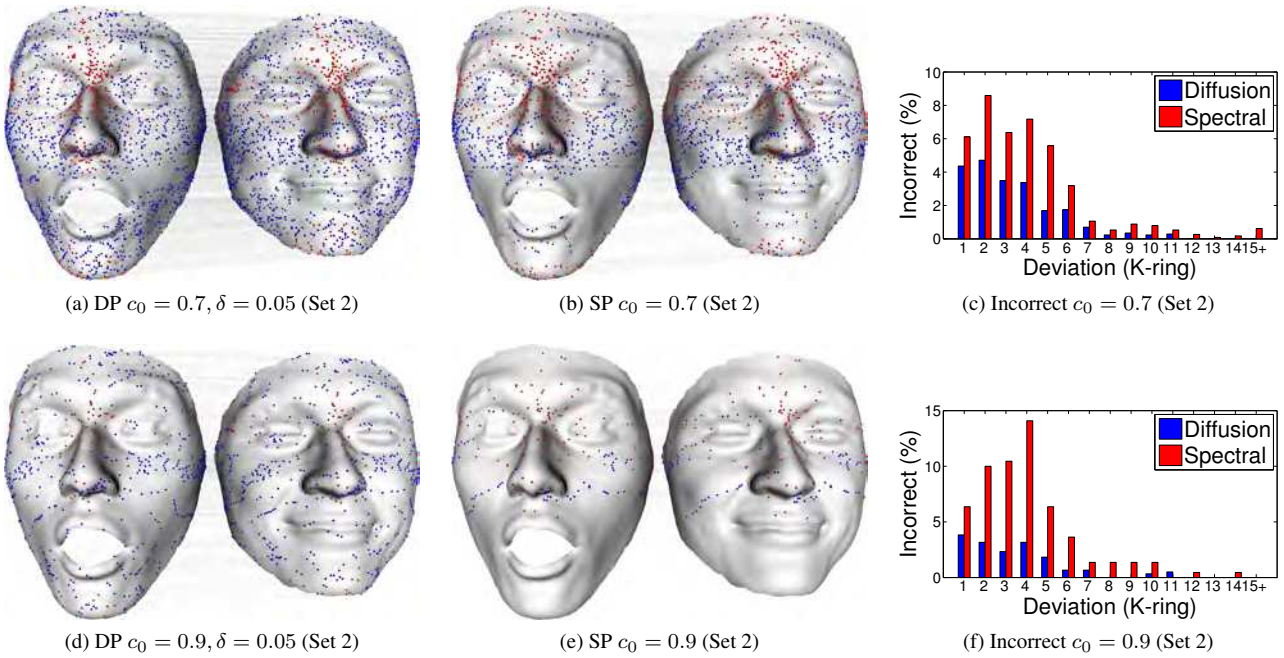

(a) DP $c_0 = 0.7, \delta = 0.05$ (Set 2) (b) SP $c_0 = 0.7$ (Set 2) (c) Incorrect $c_0 = 0.7$ (Set 2)

(d) DP $c_0 = 0.9, \delta = 0.05$ (Set 2) (e) SP $c_0 = 0.9$ (Set 2) (f) Incorrect $c_0 = 0.9$ (Set 2)

Fig. 9. Visual comparison of diffusion pruning (DP) and spectral pruning (SP) results, for faces. Globally non-isometric deformation occurs around the eyes and jaw. Blue and red dots show correct and incorrect correspondences. Histograms plot the proportion of incorrect correspondences against K-ring deviation from ground truth.

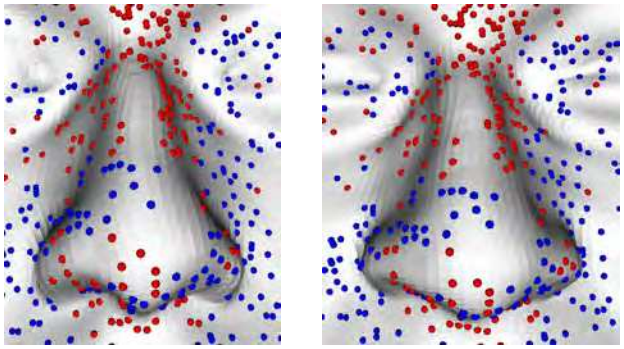

(a) Surprise (b) Smile

Fig. 10. Subtle non-isometric deformation around the nose bridge. Enlarged version of Figure 9a.

Table I. Comparison of averaged time and matrix size. (122 pairs of small models)

	Geod	1266s	Geod	19s	Geod	53s
	Matrix	21s	Matrix	7s	Matrix	13s
c_0	Total	Fill	Total	Fill	Total	Fill
0.7	1293s	50%	31s	0.4%	70s	1.4%
0.9	1291s	22%	29s	0.2%	69s	0.9%

(a) Spectral (Set 1) (b) DP $\delta = 0.05$ (c) DP $\delta = 0.1$

	Geod	1247s	Geod	19s	Geod	54s
	Matrix	21s	Matrix	7s	Matrix	13s
c_0	Total	Fill	Total	Fill	Total	Fill
0.7	1275s	55%	31s	0.4%	71s	1.7%
0.9	1273s	26%	29s	0.3%	69s	1.1%

(d) Spectral (Set 2) (e) DP $\delta = 0.05$ (f) DP $\delta = 0.1$

iments described in Sections 5.1.1, 5.1.2 and 5.2) in Tables I, II, and III respectively. A sparser matrix means a lower memory requirement; the full matrices have the same number of elements for both methods. 'Geod' is the geodesic distance pre-computation time. 'Matrix' is the time to build the sparse matrix K. 'Total' is the total time, which includes both of these and pruning time.

Geodesic distance computation was the bottleneck in both techniques. However, we reduced this bottleneck significantly by considering small geodesic discs. For small and medium-sized models with $n \approx 5000$–10000, the speed up factor was around 25–40. The advantage was even more significant for larger meshes: for $n \approx 30000$ the speed up factor was around 80–300. For spectral pruning, the experiments in Table I took 2 days for each set, while the experiment in Table III took 1 day for each set.

Note that the matrix built by spectral pruning was quite dense. For $c_0 = 0.7$ (the suggested threshold), the matrix was approximately half full. Taking the particular case in Table II (Set 2), $c_0 = 0.8$, a 37% filled sparse matrix took 5.0GB storage in Matlab. The additional memory required by the eigensolver (and other overheads) was too high for us to complete the experiments for $c_0 < 0.8$. (We used Matlab's *eigs* function, which is a variant of power iteration, in our experiment.) The matrix generated by our technique was much sparser: only 0.3% filled, requiring under 41MB storage in Matlab.

Our technique is *significantly* superior in both memory requirements and speed, and is practical on a moderate machine. With the

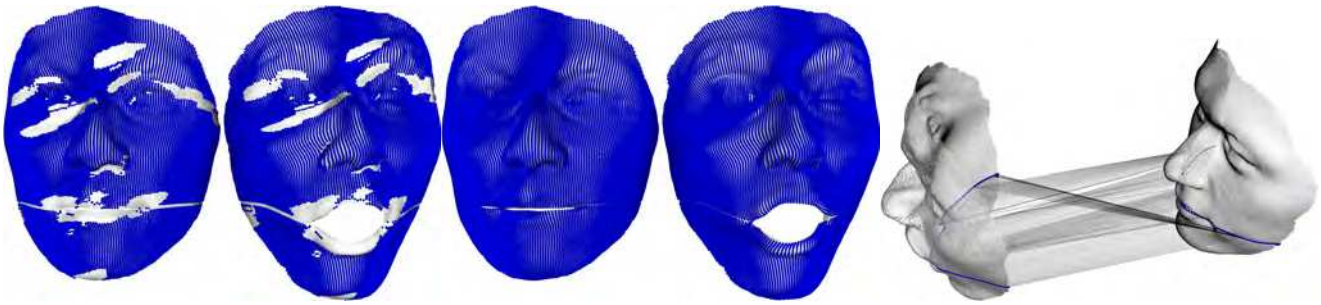

(a) $\delta = 0.05, c_0 = 0.7$ (b) $\delta = 0.05, c_0 = 0.1$ (c) Incorrect ground truth identified

Fig. 11. Analysis of non-locally isometric deformation and mislabelled vertices. Reference and surprise faces.

Table II. Comparison of time and matrix size. (Centaur)

	Geod	4595s	Geod	85s	Geod	236s
	Matrix	114s	Matrix	88s	Matrix	79s
c_0	Total	Fill	Total	Fill	Total	Fill
0.8	4851s	33%	195s	0.2%	338s	0.8%
0.9	4764s	20%	193s	0.2%	334s	0.6%

(a) Spectral (Set 1) (b) DP $\delta = 0.05$ (c) DP $\delta = 0.1$

	Geod	4598s	Geod	85s	Geod	235s
	Matrix	833s	Matrix	44s	Matrix	80s
c_0	Total	Fill	Total	Fill	Total	Fill
0.8	5534s	37%	154s	0.3%	340s	1.0%
0.9	5494s	23%	152s	0.2%	341s	1.1%

(d) Spectral (Set 2) (e) DP $\delta = 0.05$ (f) DP $\delta = 0.1$

Table III. Comparison of time and matrix size. (Face)

	Geod	69791s	Geod	148s	Geod	813s
	Matrix	15s	Matrix	24s	Matrix	46s
c_0	Total	Fill	Total	Fill	Total	Fill
0.7	69807s	58%	200s	0.4%	892s	1.3%
0.9	69806s	30%	192s	0.1%	878s	0.6%

(a) Spectral (Set 1) (b) DP $\delta = 0.05$ (c) DP $\delta = 0.1$

	Geod	72369s	Geod	157s	Geod	825s
	Matrix	14s	Matrix	24s	Matrix	45s
c_0	Total	Fill	Total	Fill	Total	Fill
0.7s	72385	63%	208s	0.3%	890s	1.5%
0.9s	72384	36%	204s	0.1%	885s	0.7%

(d) Spectral (Set 2) (e) DP $\delta = 0.05$ (f) DP $\delta = 0.1$

help of parallel processing, our technique could potentially achieve interactive speed for models of medium size.

5.4 Models with holes

Geodesic distances are affected if holes (gaps) are present in the mesh. In this section, we evaluated our technique using articulating models with multiple long holes. Long holes can be present in real data due to occlusion. In our experiments, we took a dog model and manually deleted four triangle strips on the neck, body, right back leg and left front leg. We did not remove any vertices and so retained the ground truth information. Comparative results from our method and spectral pruning are shown in Figure 13.

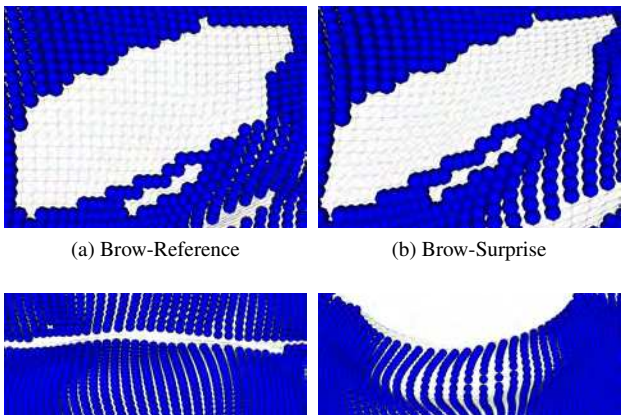

(a) Brow-Reference (b) Brow-Surprise

(c) Lip-Reference (d) Lip-Surprise

Fig. 12. c_0-locally non-isometric deformation around the brows and lip areas. (a)-(b) ($c_0 = 0.7$, local anisotropic scaling) and (c)-(d) ($c_0 = 0.1$, c.f. Figure 11a) are enlarged versions of Figure 11a and 11b respectively.

Figures 13a–13b visualise the distribution of pruned correspondences. Spectral pruning found no correspondences around the holes, while our approach of using small geodesic discs improved the robustness with respect to holes in models. Our technique resulted in a better true-positive rate than spectral pruning. Indeed, our technique was only slightly affected by the holes, as can be seen by comparison to the result without holes in Figure 13c. On the other hand, a significant accuracy drop was observed for spectral pruning. Figure 13d also indicates that the incorrect correspondences retained by our technique were much closer to ground truth.

We further tested our technique on the face model. This time, we added triangle strips to close the mouth of the smile face (Figure 7b). This is a challenging example with globally non-isometric deformation and changed connectivity. Results are shown in Figure 14. As in the earlier example in Figure 9, our technique produced better results than spectral pruning, and is unaffected by the differences in connectivity.

In both the dog and face examples our technique works because diffusion can connect good correspondences to others via regions without holes.

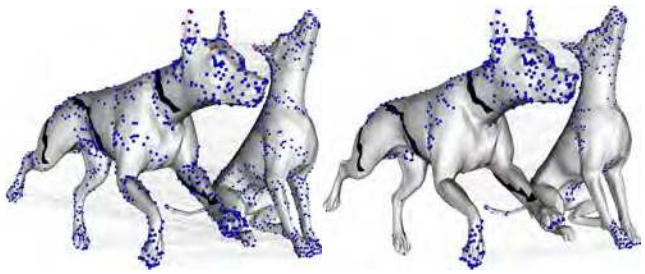

(a) DP $\delta = 0.05, c_0 = 0.7$ (b) SP $c_0 = 0.7$

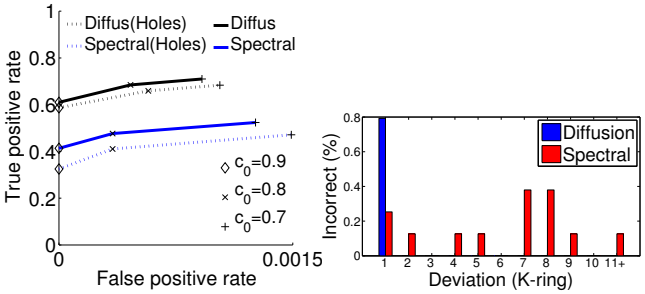

(c) ROC curves (d) Incorrect $c_0 = 0.7$

Fig. 13. Performance on models with long holes (black regions) on the neck, body, right back leg and left front leg of the left dog. Colouring of correspondences, ROC curves and histogram plots as before. (TOSCA dataset [Bronstein et al. 2008])

(a) DP $c_0 = 0.7, \delta = 0.05$ (b) SP $c_0 = 0.7$

Fig. 14. Performance on models undergoing globally non-isometric deformation with different connectivity. The mouth of the smile face (cf. Figure 7b) is closed. Colouring of correspondences as before.

5.5 Models with handles

Unlike some mapping based methods, our approach (and spectral pruning) can readily process models with through holes. Figure 15 demonstrates our technique for models with genus larger than zero. The Dragon model (10K vertices) has one handle; the Buddha model (20K vertices) has eight handles. We manually deformed the Dragon near the head and tail, and twist the Buddha near the arms. Both spectral pruning and our technique were able to retain most of the correspondences in the rigid non-deformed region. Our technique (Figures 15a and 15b) retained more correct correspondences in the non-rigidly deforming parts, as shown in Figures 15e and 15f.

(a) DP $c_0 = 0.7, \delta = 0.05$ (b) DP $c_0 = 0.7, \delta = 0.05$

(c) SP $c_0 = 0.7$ (d) SP $c_0 = 0.7$

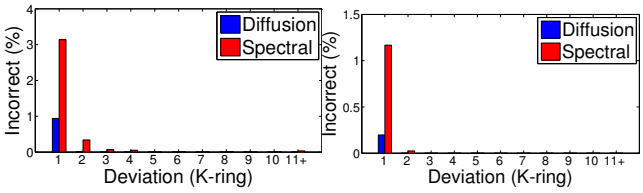

(e) Dragon (f) Buddha

Fig. 15. Visual comparison of results of diffusion pruning (DP) and spectral pruning (SP) on models with handles. The Dragon has 1 handle and the Buddha has 8 handles; both models are from [Stanford Computer Graphics Laboratory 2012]. Blue and red spheres indicate correct and incorrect correspondences. Histograms plot the percentage of incorrect correspondences against K-ring deviation from ground truth. These experiments show that our technique is applicable to high genus models.

5.6 Models with added noise

Here we evaluated our technique with different levels of noise. We introduced random noise equal to 5%, 10% and 15% of the average edge length to a cat model. As shown in Figure 16, our technique produces more correct correspondences and better coverage than spectral pruning. An example with 15% noise is shown in Figure 17.

5.7 SCAPE dataset

To test on real scanned data, we also applied our method to the SCAPE dataset [Anguelov et al. 2005]. It contains 71 human models in different poses reconstructed from scanned data. We compare diffusion pruning ($\delta = 0.05$ and $\delta = 0.1$) with spectral pruning. For each model in the dataset, another model was randomly selected. Initial correspondences between every pair of models were obtained with $|C| = 10000$ and $|G| = 1000$ (see Section 5). The threshold was chosen to be $c_0 = \{0.7, 0.85, 0.8, 0.85, 0.9, 0.95\}$ respectively and the ROC curve showing the average performance

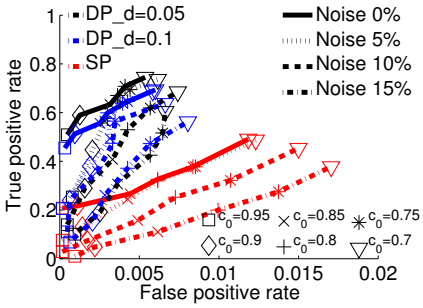

Fig. 16. Test with random noise (measured as % of average edge length) added to all vertex coordinates of a cat model.

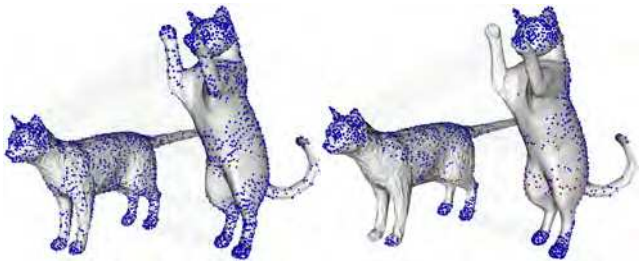

(a) DP $c_0 = 0.7, \delta = 0.05$ (b) SP $c_0 = 0.7$

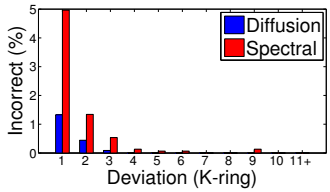

Fig. 17. Visual comparison of results of diffusion pruning (DP) and spectral pruning (SP) on models with 15% noise (TOSCA dataset [Bronstein et al. 2008]). Histograms plot the percentage of incorrect correspondences against K-ring deviation from ground truth. These experiments show that our technique is able to handle models with noise.

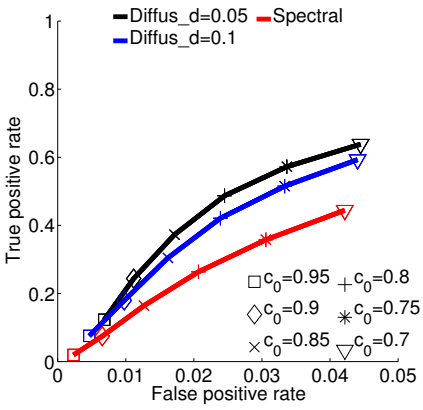

Fig. 18. ROC Evaluation on SCAPE dataset.

is shown in Figure 18. With the similarly improved efficiency (computational and memory costs), it indicates that our technique outperforms spectral pruning.

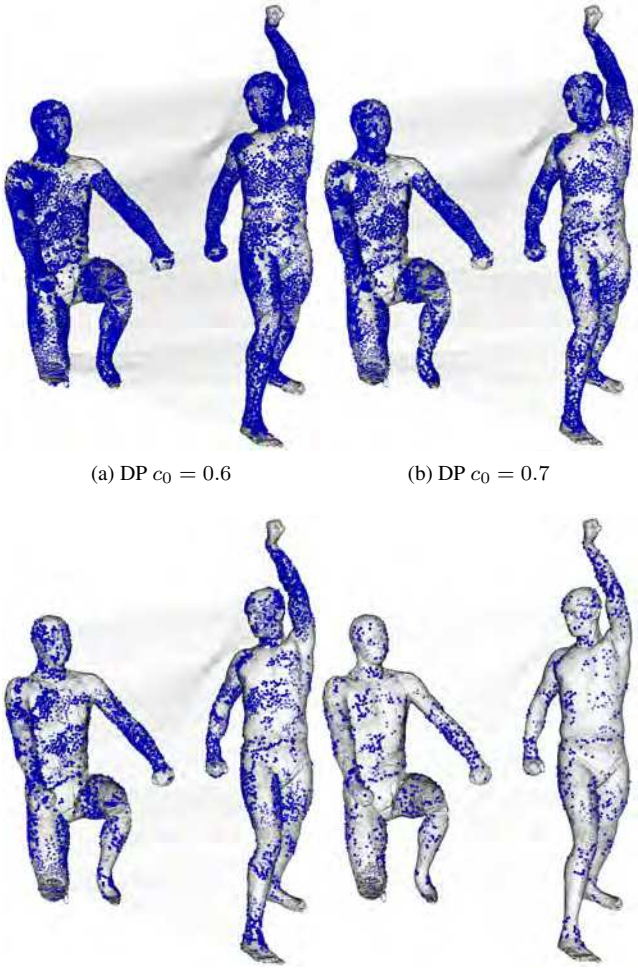

(a) DP $c_0 = 0.6$ (b) DP $c_0 = 0.7$

(c) DP $c_0 = 0.8$ (d) DP $c_0 = 0.9$

Fig. 19. Applying our technique to the results from [Kim et al. 2011] using $\delta = 0.05$ and varying c_0, SCAPE dataset [Anguelov et al. 2005]). Our technique can be quickly applied to an existing technique [Kim et al. 2011] to identify the c_0-locally isometric consistent correspondences and remove the inconsistent ones.

5.8 Application

Our technique can be applied in conjunction with the results of other correspondence establishment techniques. We show one example in Figure 19. We first obtained a blended intrinsic map using [Kim et al. 2011] between two models (12.5K vertices) from the SCAPE dataset [Anguelov et al. 2005]. We then applied our pruning technique with $\delta = 0.05$ and varying threshold c_0. Figure 19 shows that our technique can identify the c_0-locally isometric consistent correspondences and remove those that are inconsistent. The stronger the threshold, the more correspondences were pruned. Note that our technique did not require computing pairwise geodesic distances between *all* vertices. Computation took 167s for local geodesic disc computation (using a single thread for both meshes), 65s for matrix building, and 18s ($c_0 = 0.9$) to 77s ($c_0 = 0.6$) for correspondence pruning.

6. LIMITATIONS

Finding consistent correspondences between two non-rigid surfaces is related to the NP-hard quadratic assignment problem. Our technique is based on the influential work of [Huang et al. 2008], which provides an approximate solution to the NP-hard problem, and we thus share many of the limitations of that paper. Our technique is greedy in nature and may suffer from errors and cascading mistakes. If the threshold c_0 is set too high, there may be insufficient correspondences to connect all good correspondences together, leading to reduced accuracy. Our technique does not *establish* new correspondences or *interpolate* new ones. The aim of our technique is to *prune incorrect* correspondences. Therefore, we assume that the input raw correspondences contain a sufficient number of correct correspondences. If they do not, incorrect correspondences will result. To establish new correspondences from scanned data, our technique may be combined with a non-rigid registration method utilising an appropriate deformation model [Huang et al. 2008]. In this paper, we consider only one-to-one correspondences. Overcoming this restriction and extending the idea to allow neighbouring points to be matched are left as future work.

7. CONCLUSIONS

The key idea of our proposed technique is to use *local* isometry to infer *globally consistent* solutions. By restricting geodesic computations to small local discs, we show that our technique is able to relax the global isometric assumption and to handle locally isometric deformation. Our pruning technique is much faster than spectral pruning, much more memory efficient, and yet retains more correct correspondences that span a larger portion of the whole surface. Our pruning technique can be easily incorporated into registration methods, and can also be used as a valuable tool for evaluating the degree of local isometric deformation.

Acknowledgements

We thank the reviewers and editors for their insightful comments and suggestions which have improved this paper. The face mesh data [Sumner and Popović 2004] was provided by Robert Sumner and Jovan Popovic of the Computer Graphics Group at MIT. The TOSCA dataset [Bronstein et al. 2008] was provided by Alexander & Michael Bronstein. The Buddha and Dragon models were made available by the Stanford Computer Graphics Laboratory. The SCAPE dataset [Anguelov et al. 2005] was made available by James Davis of the University of California, Santa Cruz.

REFERENCES

AHUJA, R. K., MAGNANTI, T. L., AND ORLIN, J. B. 1993. *Network flows: theory, algorithms, and applications*. Prentice-Hall, Inc., Upper Saddle River, NJ, USA.

ALLEN, B., CURLESS, B., AND POPOVIĆ, Z. 2003. The space of human body shapes: reconstruction and parameterization from range scans. In *Proc. ACM SIGGRAPH*. 587–594.

ANGUELOV, D., SRINIVASAN, P., KOLLER, D., THRUN, S., RODGERS, J., AND DAVIS, J. 2005. SCAPE: shape completion and animation of people. *ACM Trans. on Graphics 24,* 3, 408–416.

ANGUELOV, D., SRINIVASAN, P., PANG, H.-C., KOLLER, D., THRUN, S., AND DAVIS, J. 2004. The correlated correspondence algorithm for unsupervised registration of nonrigid surfaces. *Neural Info. Process. Sys. 17*, 33–40.

BESL, P. J. AND MCKAY, N. D. 1992. A method for registration of 3-d shapes. *IEEE Trans. Pat. Anal. & Mach. Intell. 14,* 2, 239–256.

BOKELOH, M., BERNER, A., WAND, M., SCHILLING, A., AND SEIDEL, H.-P. 2008. Slippage features. Tech. rep., University of Tübingen. Technical Report, WSI-2008-03.

BRONSTEIN, A. M., BRONSTEIN, M. M., AND KIMMEL, R. 2006. Generalized multidimensional scaling: A framework for isometry-invariant partial surface matching. *Proc. of Nat. Acad. of Sci. 103,* 5, 1168–1172.

BRONSTEIN, A. M., BRONSTEIN, M. M., AND KIMMEL, R. 2008. *Numerical geometry of non-rigid shapes*. Springer Verlag, New York, USA.

BRONSTEIN, A. M., BRONSTEIN, M. M., KIMMEL, R., MAHMOUDI, M., AND SAPIRO, G. 2010. A Gromov-Hausdorff framework with diffusion geometry for topologically-robust non-rigid shape matching. *Int. J. Comp. Vis. 89,* 2-3, 266–286.

BROWN, B. J. AND RUSINKIEWICZ, S. 2007. Global non-rigid alignment of 3-D scans. *ACM Trans. on Graphics 26,* 3, 21:1–21:9.

CHANG, K. I., BOWYER, K. W., AND FLYNN, P. J. 2006. Multiple nose region matching for 3D face recognition under varying facial expression. *IEEE Trans. Pat. Anal. & Mach. Intell. 28,* 10, 1695–1700.

CHANG, W., LI, H., MITRA, N. J., PAULY, M., RUSINKIEWICZ, S., AND WAND, M. 2011. Computing correspondences in geometric data sets. In *Eurographics 2011 tutorial*.

CHANG, W. AND ZWICKER, M. 2008. Automatic registration for articulated shapes. *Comp. Graphics Forum 27,* 5, 1459–1468.

CHANG, W. AND ZWICKER, M. 2009. Range scan registration using reduced deformable models. *Comp. Graphics Forum 28,* 2, 447–456.

CHEN, Y. AND MEDIONI, G. 1991. Object modeling by registration of multiple range images. In *Proc. Int. Conf. Robotics and Automation*. Vol. 3. 2724–2729.

CHERTOK, M. AND KELLER, Y. 2010. Spectral symmetry analysis. *IEEE Trans. Pat. Anal. & Mach. Intell. 32,* 7, 1227–1238.

CHUNG, F. R. K. 1997. *Spectral Graph Theory*. AMS & CBMS, USA.

COIFMAN, R. R. AND LAFON, S. 2006. Diffusion maps. *Applied and Computational Harmonic Analysis 21,* 1, 5–30.

DEZSO, B., JÜTTNER, A., AND KOVÁCS, P. 2011. LEMON - an open source C++ graph template library. *Electronic Notes in Theoretical Comp. Sci. 264,* 5, 23–45.

EGOZI, A., KELLER, Y., AND GUTERMAN, H. 2013. A probabilistic approach to spectral graph matching. *IEEE Trans. Pat. Anal. & Mach. Intell. 35,* 1, 18–27.

FORSYTH, D. A. AND PONCE, J. 2002. *Computer Vision: A Modern Approach*. Prentice Hall, USA.

FOUSS, F., PIROTTE, A., RENDERS, J.-M., AND SAERENS, M. 2007. Random-walk computation of similarities between nodes of a graph with application to collaborative recommendation. *IEEE Trans. Knowledge and Data Engineering 19*, 355–369.

FUNKHOUSER, T. AND SHILANE, P. 2006. Partial matching of 3D shapes with priority-driven search. In *Proc. Euro. Symp. on Geom. Process.* 131–142.

GAL, R. AND COHEN-OR, D. 2006. Salient geometric features for partial shape matching and similarity. *ACM Trans. on Graphics 25,* 1, 130–150.

GARLAND, M. AND HECKBERT, P. S. 1997. Surface simplification using quadric error metrics. In *Proc. ACM SIGGRAPH*. 209–216.

GELFAND, N., MITRA, N. J., GUIBAS, L. J., AND POTTMANN, H. 2005. Robust global registration. In *Proc. Euro. Symp. on Geom. Process.* 197–206.

HILAGA, M., SHINAGAWA, Y., KOHMURA, T., AND KUNII, T. L. 2001. Topology matching for fully automatic similarity estimation of 3D shapes. In *Proc. ACM SIGGRAPH*. 203–212.

HUANG, Q.-X., ADAMS, B., WICKE, M., AND GUIBAS, L. J. 2008. Non-rigid registration under isometric deformations. *Comp. Graphics Forum 27,* 5, 1449–1457.

JAIN, V. AND ZHANG, H. 2006. Robust 3D shape correspondence in the spectral domain. In *Proc. IEEE Conf. on Shape Modeling and Applications*. 118–129.

JOHNSON, A. E. AND HEBERT, M. 1999. Using spin images for efficient object recognition in cluttered 3D scenes. *IEEE Trans. Pat. Anal. & Mach. Intell. 21,* 5, 433–449.

KIM, V., LIPMAN, Y., AND FUNKHOUSER, T. 2011. Blended intrinsic maps. *ACM Trans. on Graphics 30,* 4, 79:1–79:12.

KIM, V. G., LI, W., MITRA, N. J., DIVERDI, S., AND FUNKHOUSER, T. 2012. Exploring collections of 3D models using fuzzy correspondences. *ACM Trans. on Graphics 31,* 4 (July), 54:1–54:11.

KOVNATSKY, A., BRONSTEIN, M. M., BRONSTEIN, A. M., GLASHOFF, K., AND KIMMEL, R. 2013. Coupled quasi-harmonic bases. *Comp. Graphics Forum 32,* 2pt4, 439–448.

LAFON, S. AND LEE, A. 2006. Diffusion maps and coarse-graining: a unified framework for dimensionality reduction, graph partitioning, and data set parameterization. *IEEE Trans. Pat. Anal. & Mach. Intell. 28,* 9, 1393–1403.

LEORDEANU, M. AND HEBERT, M. 2005. A spectral technique for correspondence problems using pairwise constraints. In *Proc. Int. Conf. on Comp. Vis.* Vol. 2. 1482–1489.

LEORDEANU, M., SUKTHANKAR, R., AND HEBERT, M. 2012. Unsupervised learning for graph matching. *Int. J. Comp. Vis. 96*, 28–45.

LI, H., ADAMS, B., GUIBAS, L. J., AND PAULY, M. 2009. Robust single-view geometry and motion reconstruction. *ACM Trans. on Graphics 28,* 5, 175:1–175:10.

LI, H., SUMNER, R. W., AND PAULY, M. 2008. Global correspondence optimization for non-rigid registration of depth scans. *Comp. Graphics Forum 27,* 5, 1421–1430.

LIPMAN, Y., CHEN, X., DAUBECHIES, I., AND FUNKHOUSER, T. 2010. Symmetry factored embedding and distance. *ACM Trans. on Graphics 29,* 4, 103:1–103:12.

LIPMAN, Y. AND FUNKHOUSER, T. 2009. Möbius voting for surface correspondence. *ACM Trans. on Graphics 28,* 3, 72:1–72:12.

LIPMAN, Y., RUSTAMOV, R. M., AND FUNKHOUSER, T. A. 2010. Biharmonic distance. *ACM Trans. on Graphics 29,* 3, 27:1–27:11.

MATEUS, D., HORAUD, R., KNOSSOW, D., CUZZOLIN, F., AND BOYER, E. 2008. Articulated shape matching using Laplacian eigenfunctions and unsupervised point registration. In *Proc. IEEE Conf. CVPR*. 1–8.

MÉMOLI, F. 2011. A spectral notion of gromov-wasserstein distance and related methods. *Applied and Comp. Harmonic Anal. 30,* 3, 363–401.

OVSJANIKOV, M., BEN-CHEN, M., SOLOMON, J., BUTSCHER, A., AND GUIBAS, L. 2012. Functional maps: A flexible representation of maps between shapes. *ACM Trans. on Graphics 31,* 4 (July), 30:1–30:11.

OVSJANIKOV, M., MÉRIGOT, Q., MÉMOLI, F., AND GUIBAS, L. J. 2010. One point isometric matching with the heat kernel. *Comp. Graphics Forum 29,* 5, 1555–1564.

PAULY, M., MITRA, N. J., GIESEN, J., GROSS, M., AND GUIBAS, L. J. 2005. Example-based 3D scan completion. In *Proc. Euro. Symp. on Geom. Process.* 23–32.

PEYRÉ, G. AND COHEN, L. D. 2006. Geodesic remeshing using front propagation. *Int. J. Comp. Vis. 69,* 1, 145–156.

POKRASS, J., BRONSTEIN, A. M., BRONSTEIN, M. M., SPRECHMANN, P., AND SAPIRO, G. 2013. Sparse modeling of intrinsic correspondences. *Comp. Graphics Forum 32,* 2pt4, 459–468.

ROSMAN, G., BRONSTEIN, M. M., BRONSTEIN, A. M., AND KIMMEL, R. 2010. Nonlinear dimensionality reduction by topologically constrained isometric embedding. *Int. J. Comp. Vis. 89,* 1, 56–68.

SAHILLIOGLU, Y. AND YEMEZ, Y. 2011. Coarse-to-fine combinatorial matching for dense isometric shape correspondence. *Comp. Graphics Forum 30,* 5, 1461–1470.

SHARMA, A. AND HORAUD, R. 2010. Shape matching based on diffusion embedding and on mutual isometric consistency. In *Proc. IEEE Conf. CVPR Workshop*. 29–36.

SIDI, O., VAN KAICK, O., KLEIMAN, Y., ZHANG, H., AND COHEN-OR, D. 2011. Unsupervised co-segmentation of a set of shapes via descriptor-space spectral clustering. *ACM Trans. on Graphics 30,* 6, 126:1–126:10.

Stanford Computer Graphics Laboratory 2012. The Stanford 3D Scanning Repository. `http://graphics.stanford.edu/data/3Dscanrep/`.

SUMNER, R. W. AND POPOVIĆ, J. 2004. Deformation transfer for triangle meshes. In *Proc. ACM SIGGRAPH*. 399–405.

SUN, J., CHEN, X., AND FUNKHOUSER, T. 2010. Fuzzy geodesics and consistent sparse correspondences for deformable shapes. *Comp. Graphics Forum 29,* 5, 1535–1544.

SUN, J., OVSJANIKOV, M., AND GUIBAS, L. J. 2009. A concise and provably informative multi-scale signature based on heat diffusion. In *Proc. Euro. Symp. on Geom. Process.* 1383–1392.

SURAZHSKY, V., SURAZHSKY, T., KIRSANOV, D., GORTLER, S. J., AND HOPPE, H. 2005. Fast exact and approximate geodesics on meshes. *ACM Trans. on Graphics 24,* 3, 553–560.

TAM, G. K., CHENG, Z.-Q., LAI, Y.-K., LANGBEIN, F., LIU, Y., MARSHALL, A. D., MARTIN, R. R., SUN, X., AND ROSIN, P. L. 2013. Registration of 3D point clouds and meshes: A survey from rigid to non-rigid. *IEEE Trans. Vis. & Comp. Graphics 19,* 7, 1199–1217.

TEVS, A., BERNER, A., WAND, M., IHRKE, I., AND SEIDEL, H.-P. 2011. Intrinsic shape matching by planned landmark sampling. *Comp. Graphics Forum 30,* 2, 543–552.

TEVS, A., BOKELOH, M., WAND, M., SCHILLING, A., AND SEIDEL, H.-P. 2009. Isometric registration of ambiguous and partial data. In *Proc. IEEE Conf. CVPR*. 1185–1192.

TOMBARI, F., SALTI, S., AND DI STEFANO, L. 2010. Unique signatures of histograms for local surface description. In *Proc. Euro. Conf. on Comp. Vis.* Vol. 6313. 356–369.

VAN KAICK, O., ZHANG, H., HAMARNEH, G., AND COHEN-OR, D. 2011. A survey on shape correspondence. *Comp. Graphics Forum 30,* 6, 1681–1707.

VLASIC, D., BRAND, M., PFISTER, H., AND POPOVIĆ, J. 2004. Multilinear models for face synthesis. In *ACM SIGGRAPH Sketches*. 56.

ZHANG, H., SHEFFER, A., COHEN-OR, D., ZHOU, Q., VAN KAICK, O., AND TAGLIASACCHI, A. 2008. Deformation-driven shape correspondence. *Comp. Graphics Forum 27,* 5, 1431–1439.

ZHENG, Q., SHARF, A., TAGLIASACCHI, A., CHEN, B., ZHANG, H., SHEFFER, A., AND COHEN-OR, D. 2010. Consensus skeleton for non-rigid space-time registration. *Comp. Graphics Forum 29,* 2, 635–644.

Received May 2012; accepted June 2013